AD-A074 098 KENTUCKY UNIV LEXINGTON DEPT OF ENGINEERING MECHANICS F/G 20/11
THERMO-MECHANICAL STRESS ANALYSIS OF ADVANCED TURBINE BLADE COO--ETC(U)
JUL 79 F J RIZZO, D J SHIPPY AFOSR-75-2824

UNCLASSIFIED UKY-TR111-79-EM17 AFOSR-TR-79-0953 NL

| OF |
ADA
074098

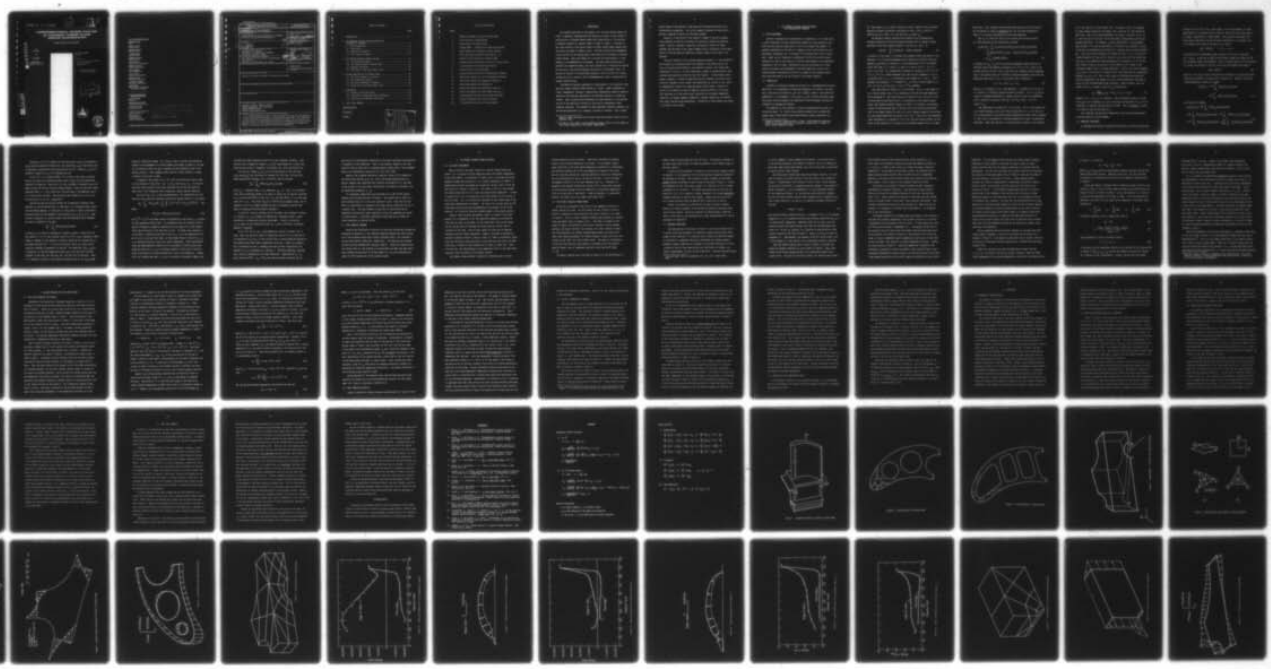

END
DATE
FILMED
10-79
DDC

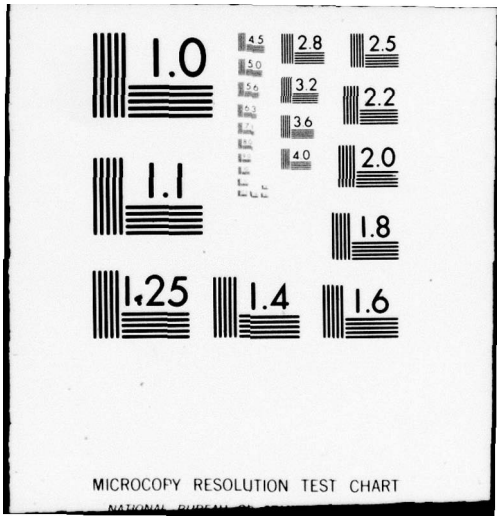
1.0
1.1
1.25
1.4
1.6
1.8
2.0
2.2
2.5
2.8
3.2
3.6
4.0
4.5
5.0
5.6
MICROCOPY RESOLUTION TEST CHART

THERMOMECHANICAL STRESS ANALYSIS OF ADVANCED TURBINE BLADE COOLING CONFIGURATION

FINAL SCIENTIFIC REPORT

by
F.J. Rizzo

and

D.J. Shippy

Department of
Engineering Mechanics

UKY TR111-79-EM17
July 1979

Prepared for:

Air Force Office of Scientific Research
Bolling Air Force Base
Washington, D. C.

Approved for Public Release
Distribution Unlimited

UNIVERSITY OF KENTUCKY ENGINEERING

UNIVERSITY OF KENTUCKY 18 65 UNITED WE STAND DIVIDED WE FALL

For additional copies of information address correspondence to:

ORES Publications
College of Engineering
University of Kentucky
Lexington, Kentucky 40506

A PUBLICATION OF THE OFFICE OF RESEARCH AND ENGINEERING SERVICES

UNCLASSIFIED

SECURITY CLASSIFICATION OF THIS PAGE *(When Data Entered)*

REPORT DOCUMENTATION PAGE	READ INSTRUCTIONS BEFORE COMPLETING FORM
1. REPORT NUMBER: AFOSR-TR-79-0953	2. GOVT ACCESSION NO. / 3. RECIPIENT'S CATALOG NUMBER
4. TITLE *(and Subtitle)*: THERMO-MECHANICAL STRESS ANALYSIS OF ADVANCED TURBINE BLADE COOLING CONFIGURATION.	5. TYPE OF REPORT & PERIOD COVERED: FINAL rept. 1 MAY 1975 — 15 JULY 1979
	6. PERFORMING ORG. REPORT NUMBER: UKY-TR111-79-EM17
7. AUTHOR(s): F. J. RIZZO, D. J. SHIPPY	8. CONTRACT OR GRANT NUMBER(s): AFOSR-75-2824
9. PERFORMING ORGANIZATION NAME AND ADDRESS: UNIVERSITY OF KENTUCKY, DEPARTMENT OF ENGINEERING MECHANICS, LEXINGTON, KENTUCKY 40506	10. PROGRAM ELEMENT, PROJECT, TASK AREA & WORK UNIT NUMBERS: 61102F, 2307, B1
11. CONTROLLING OFFICE NAME AND ADDRESS: AIR FORCE OFFICE OF SCIENTIFIC RESEARCH/NA, BUILDING 410, BOLLING AIR FORCE BASE, D.C. 20332	12. REPORT DATE: JULY 1979 / 13. NUMBER OF PAGES: 63
14. MONITORING AGENCY NAME & ADDRESS *(if different from Controlling Office)*	15. SECURITY CLASS. *(of this report)*: UNCLASSIFIED / 15a. DECLASSIFICATION/DOWNGRADING SCHEDULE

16. DISTRIBUTION STATEMENT *(of this Report)*

Approved for public release; distribution unlimited.

17. DISTRIBUTION STATEMENT *(of the abstract entered in Block 20, if different from Report)*

18. SUPPLEMENTARY NOTES

19. KEY WORDS *(Continue on reverse side if necessary and identify by block number)*

BOUNDARY INTEGRAL EQUATION METHOD
THERMO-MECHANICAL STRESS ANALYSIS
STRESS CONCENTRATION
TURBINE BLADE COOLING HOLE

20. ABSTRACT *(Continue on reverse side if necessary and identify by block number)*

A thermo-mechanical stress analysis capability, based on the Boundary Integral Equation Method (BIE) is developed and described. The capability is used to provide a thermoelastic analysis of stress in the vicinity of cooling holes in turbojet engine blades with transpiration or film cooling. Details involved in the formulation, numerical procedures, mathematical modelling, and data from solved problems are presented.

DD FORM 1 JAN 73 1473 EDITION OF 1 NOV 65 IS OBSOLETE

UNCLASSIFIED 403 077

SECURITY CLASSIFICATION OF THIS PAGE *(When Data Entered)*

TABLE OF CONTENTS

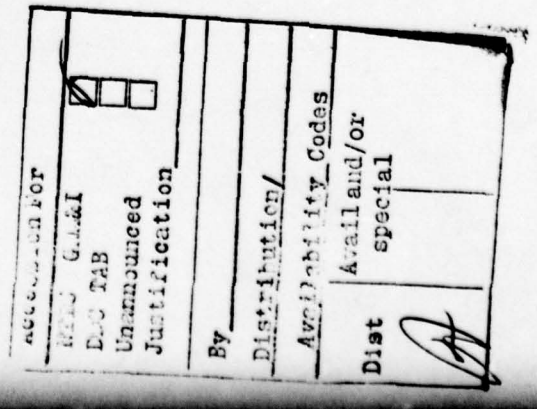

LIST OF ILLUSTRATIONS

1. INTRODUCTION

The research described in this report, (cf. previous interim reports [1, 2,3]), is generally concerned with the analysis of stress in the vicinity of cooling holes in turbojet engine blades with transpiration or film cooling. A schematic diagram of a typical blade[1] is shown in Figure 1. Portions of the cross-sections of two typical types of blades (taken midway between cooling holes) are shown in Figures 2 and 3. Possible cooling hole arrangements in the vicinity of the leading edge of the blade are as indicated in the mentioned Figures. When such blades are in service the blade material is subjected to a thermomechanical environment. The outer blade surfaces are in contact[2] with combustion gases, the inner surfaces are in contact with cooling air, and spin of the turbine subjects the blade to a centrifugal field. Of particular interest in the described research is the "vicinity" of a single cooling hole (e.g. Figure 4) where thermomechanical stress concentrations of present interest occur.

The method of analysis employed for investigation of this problem is the Boundary Integral Equation (BIE) method (cf. [4,5]). Under assumptions of linear, homogeneous, isotropic, steady-state, thermoelastic material behavior, analytical BIE relations applicable to an arbitrary portion of a blade are written. Next, discretization assumptions are made leading to a discretized version of the analytical relations in the form of simultaneous linear algebraic equations. The unknowns in these equations, generally speaking, are the desired quantities, e.g. stresses, at points of interest. Thus a mathe-

---

[1] Specific blade configurations and data supplied by General Electric (G.E.), Evendale, Ohio.

[2] All data in this report, unless otherwise stated, refer to first stage turbine blades subjected to the highest temperatures.

matical model of the problem is made under the indicated constitutive and discretization assumptions. Our various computer programs are then used to provide a numerical solution to this model problem.

Actually, in the course of the research a number of specific boundary value problems for specific facsimiles of portions of blades are posed and solved. Details, rationale, discussion, and specific results for these problems form the body of this report together with a discussion of the latest version of the BIE analysis capability created largely for and used in our analyses.

The basic integrity of our working computer programs, i.e. the reliability and accuracy to be expected within the framework of the theory versus the level of discretization needed for the numerical analysis, has largely been established in [1,2,3]. In those references a number of representative "test" problems were posed and solved for just this purpose. In the present report, however, emphasis is placed on modelling specific problems, the results from which are intended to give insight into mechanisms for, causes of, and levels of thermoelastic stress in an advanced design turbine blade. Accuracy of results as a function of level of numerical analysis effort is not so much the issue here as is the reality and reliability of the models themselves, especially as regards symmetry assumptions, boundary conditions, and thermal data input from the blade manufacturer. Discussion of these matters and others is included in this report.

2. THE BOUNDARY INTEGRAL EQUATION METHOD FOR THERMOELASTIC PROBLEMS

2.1 BRIEF BACKGROUND

The BIE is becoming well established as a companion to, or in some cases, a viable alternative for more conventional methods of stress analysis, principal and most familiar among which is the Finite Element (FE) method. An extensive background for the BIE or a lengthy a-priori justification for its employment, advantages, etc. in problems of the present type is out of place here. Rather we call attention to references [4,9,15,16] as fairly recent indicators of some of the features of the BIE, some aspects of its analytical foundations, and its scope. References [1,2,3,5,13,14] record to a large extent the progress and development of the BIE capability as used in the present context including the solution of a number of test problems some of which were motivated by and are related to the present research.

2.2 FORMULATION

Consider an arbitrarily shaped solid body B in a thermomechanical environment which, as a consequence of conditions imposed on its surface S and possibly a body force distribution b_i per unit volume[3], suffers a distribution of temperature θ, displacement u_i, and stress σ_{ij} from a uniform reference state. The stress, the displacement, and temperature fields throughout the body are frequently of engineering interest.

The approach to such problems in classical thermoelasticity usually involves two steps: (1) Solve a heat transfer problem first to obtain the steady state θ field based on well-posed thermal boundary conditions on S.

---

[3] Standard Cartesian Tensor Analysis is used. Latin subscripts have the range 1,2 or 1,2,3 according as B occupies, respectively, a region of two or three-dimensional space.

(2) Then regard $\theta_{,i}$ as a type of body force which, together with well-posed mechanical boundary conditions, contributes to the u_i and σ_{ij} field in a familiar way (e.g. [6] p. 77), and solve for u_i and/or σ_{ij}.

The Boundary Integral Equation (BIE) method for such thermoelastic problems recognizes the above two steps and begins with an integral formula pertinent to the heat transfer problem in the form (cf. [4] p. 1):

$$c(p)\theta(p) = \int_S [\theta'(Q)K(p,Q) - \theta(Q)K'(p,Q)]dS(Q). \qquad (1)$$

In formula (1) the prime (') indicates the (outward) normal derivative of the function, K is a two-point-dependent kernel function of differing form (see Appendix) according as B pertains to a three-dimensional (E^3) or two-dimensional (E^2) body, Q is a point ε S, and p is a point ε B or S. If p ε B, $c(p) = 4\pi$ or $c(p) = 2\pi$, respectively, according as the body B ε E^3 or B ε E^2. If p ε S, c(p) is a number dependent only upon the local geometry of S at p. In practice c(p), p ε S, is calculated as the integral of K' over S. This is apparent from setting $\theta \equiv 1$ in formula (1). If S has a unique tangent at p, $c(p) = 2\pi$ for B ε E^3 and $c(p) = \pi$ for B ε E^2 as expected.

The significance of formula (1) is as follows. Let p ε S and regard (1) as a relation among θ and θ' on S pertaining to one and the same temperature field throughout B. Now since only part of the pair (θ,θ') (e.g. θ or θ' but not both) may be specified at any Q ε S according to a well-posed, steady state, heat transfer problem, formula (1) with p ε S provides, in principle, a means of obtaining that part of the pair (θ,θ') not initially prescribed. That is, we regard formula (1) with p ε S as an integral equation to be solved for the unprescribed parts of the pair (θ,θ') on S. Once (θ,θ') are completely known everywhere on S, consider p ε B in (1), and that formula yields θ at any point in the interior of B in terms of the indicated integral over S of known

quantities. Thus, assuming the above-described process can be carried out, and the method for doing so <u>numerically</u> will be indicated subsequently, Step (1) in classical thermoelasticity has been completed.

Step (2) is similar to Step (1) and involves the following formula (cf. [5]) pertinent to the thermoelastic problem:

$$c_{ij}(p)u_i(p) = \int_S [\{t_i(Q)-\psi(Q)n_i(Q)\}U_{ij}(p,Q)-u_i(Q)T_{ij}(p,Q)]dS(Q)$$
$$+ \int_S [\{\psi(Q)+\gamma\theta(Q)\}W'_{,j}(p,Q) - \{\psi(Q)+\gamma\theta(Q)\}'W_{,j}(p,Q)]dS(Q)$$
$$+ k_o \int_S n_j(Q)W(p,Q)dS(Q). \qquad (2)$$

In formula (2) U_{ij}, T_{ij} and W are two-point-dependent kernel functions of differing forms (see Appendix) according as $B \in E^3$ or $B \in E^2$, $t_i(Q)$ is the surface traction, $r(p,Q) \equiv |Q-p|$, $n_j(Q)$ are unit (outward) normal components, $\psi(Q)$ is the surface value of a function ψ defined throughout B such that the mechanical body force, if any, is derivable from ψ according to

$$b_i = -\psi_{,i} \quad \text{with} \quad \psi_{,ii} = k_o, \qquad (3)$$

where k_o is a constant, as is γ (see Appendix). In formula (2) p may be $\in$ B or S and the (') signifies normal derivative as before. If $p \in S$, $c_{ij}(p)$ is a matrix of numbers determined in a manner similar to that for determining c(p) in formula (1) (see e.g. [5], Eqs. (1), (14), (15)). If $p \in B$, $c_{ij}(p) \equiv \delta_{ij}$.

The significance of formula (2) is as follows. Let $p \in S$ and regard (2) as a relation among u_i and t_i on S and the functions θ, θ', ψ, ψ' also on S, all of which pertain to one and the same thermoelastic stress state throughout B. Now θ and θ' are known on S following completion of step 1 as previously described. (Note that setting $p \in B$ and solving for interior θ with formula

(1) is not required in using formula (2)). Variables ψ and ψ' are regarded as known boundary quantities obtainable from a potential for real mechanical body force. What is not known completely, of course, is the pair (u_i,t_i) on S, since only part of the pair can be prescribed corresponding to well-posed boundary conditions. For example, u_i may be prescribed on S (displacement type problem), or t_i may be prescribed on S (traction type problem), or parts of each may be prescribed over portions of S (various kinds of mixed problems), etc. Thus, the solution strategy via formula (2) with $p \in S$ is to solve the integral equation for that part of the pair (u_i,t_i) not initially prescribed. Once (u_i,t_i) are completely known everywhere on S, consider $p \in B$ in (2) and that formula yields u_i at any point in the interior of B in terms of the indicated integrals over S of known quantities. Finally, the stress components σ_{ij} at any $p \in B$ are given via formula (2) by first obtaining the displacement gradient $u_{i,k}$ at $p \in B$. This is done simply by differentiating the kernel function expressions with respect to x_k at p and evaluating the indicated integrals of the differentiated kernel functions. Based on Hooke's Law, the stress field σ_{ij} is given in terms of $u_{i,j}$ according to

$$\sigma_{ij} = \frac{2\mu\nu}{1-2\nu} u_{m,m}\delta_{ij} + \mu[u_{i,j} + u_{j,i}] - \delta_{ij}\gamma\theta \qquad (4)$$

wherein $p \in B$. If σ_{ij} on S is desired, it may be obtained directly in terms of (θ,u_i,t_i) on S (actually θ,t_i and "in-surface" derivative(s) of u_i on S are required) in a familiar fashion (see e.g. [7,8]). Thus for <u>surface</u> σ_{ij} there is no need to refer to the interior p.

This completes the analytical formulation of the two-step thermoelastic solution process via the BIE method.

2.3 NUMERICAL PROCEDURES

To implement the solution strategy outlined above, we first discretize the

surface S of B, B ε E^3, into a total number m of surface elements of either quadrilateral or triangular shape as shown in Figure 5(a) and locate eight or six nodes, respectively, on each element. The cartesian coordinates x_i^α of each node are specified, and the cartesian coordinates of a non-nodal point of an element are assumed to be given by (cf. [5,9])

$$x_i(\xi) = M^\alpha(\xi)x_i^\alpha \qquad \alpha = 1,2\ldots,6 \text{ or } 8 \tag{5}$$

in which $M^\alpha(\xi)$ are second-order shape functions of intrinsic coordinates $(\xi) \equiv (\xi_1\xi_2)$. We use one set M_R^α for quadrilateral shapes and another set M_T^α for triangular shapes (see Appendix). Next, we assume that any of the functions of Q alone in equations (1) and (2) varies over the elements according to

$$\phi(\xi) = M^\alpha(\xi)\phi^\alpha \tag{6}$$

where ϕ^α is the nodal value of the particular variable at issue and the shape functions are identical to those used in equation (5). Based on the discretizing assumptions, formula (1) becomes

$$c(P_\eta)\theta(P_\eta) = \theta'^{\alpha\sigma}\int_{S_\sigma} M(\xi)K(P_\eta,Q(\xi))J(\xi)d\xi$$

$$- \theta^{\alpha\sigma}\int_{S_\sigma} M(\xi)K'(P_\eta,Q(\xi))J(\xi)d\xi \tag{7}$$

and formula (2) becomes

$$c_{ij}(P_\eta)u_i(P_\eta) = \Omega_i^{\alpha\sigma}\int_{S_\sigma} M^\alpha(\xi)U_{ij}(P_\eta,Q(\xi))J(\xi)d\xi$$

$$- u_i^{\alpha\sigma}\int_{S_\sigma} M^\alpha(\xi)T_{ij}(P_\eta,Q(\xi))J(\xi)d\xi + T^{\alpha\sigma}\int_{S_\sigma} M^\alpha(\xi)W',_j(P_\eta,Q(\xi))J(\xi)d\xi$$

$$- T'^{\alpha\sigma}\int_{S_\sigma} M^\alpha(\xi)W,_j(P_\eta,Q(\xi))J(\xi)d\xi + k_o\sum_{\sigma=1}^{m}\int_{S_\sigma} n_j(Q(\xi))W(P_\eta,Q(\xi))J(\xi)d\xi \tag{8}$$

in which it is assumed $p \equiv P \in S$, and in which $\Omega_i = t_i - \psi n_i$; $T \equiv \psi + \gamma\theta$; and where the quantities $\phi^{\alpha\sigma}$ have the meaning "the value of ϕ at local node α on surface element S_σ". Note that $\sigma = 1,2,\ldots, m$ and $\eta = 1,2,\ldots, n$, where n is the total number of nodes; summation is implied on all repeated subscripts; $J(\xi)$ is simply the ratio $dS(Q)/d\xi$, which more explicitly is

$$J(\xi) = |\underset{\sim}{a}_1 \times \underset{\sim}{a}_2| \tag{9}$$

where the components of the vectors $\underset{\sim}{a}_\mu$ in the cross product are given by

$$a_{\mu i} \equiv \frac{\partial M^\alpha}{\partial \xi_\mu} x_i^\alpha. \tag{10}$$

Note that since a node always lies on at least two surface elements and frequently more, $\phi^{\alpha\sigma}$ is the same quantity for several sets of values of α and σ. This little bookkeeping problem, when addressed, leads to viewing the system of equations (7) and (8) in the following matrix forms, respectively:

$$\underset{\sim\sim}{F}\underset{\sim}{\theta} = \underset{\sim\sim}{G}\underset{\sim}{\theta}' \tag{11}$$

$$\underset{\sim\sim}{A}\underset{\sim}{u} - \underset{\sim\sim}{B}\underset{\sim}{\Omega} = \underset{\sim\sim}{C}\underset{\sim}{T} - \underset{\sim\sim}{D}\underset{\sim}{T}' + \underset{\sim}{E}. \tag{12}$$

In equation (11) the column matrices $\underset{\sim}{\theta}$ and $\underset{\sim}{\theta}'$ are n elements long and contain the elements θ^β, θ'^β, $\beta = 1,2,\ldots n$, which are, respectively, temperature and normal derivative of temperature at global node number β. The square matrices $\underset{\sim}{F}$ and $\underset{\sim}{G}$ are $n \times n$ in size and contain the integral coefficients (and the $c(P_\eta)$ term) as indicated in equation (7).

In equation (12), the column matrices $\underset{\sim}{u}$ and $\underset{\sim}{\Omega}$ are 3n elements long and contain the elements u_i^β, Ω_i^β, $\beta = 1,2,\ldots, n$, which are, respectively, displacement and "augmented" traction components at global number β; $\underset{\sim}{T}$ and $\underset{\sim}{T}'$ are n elements long and contain T^β, T'^β, i.e., the surface contribution of temperature and body force potential and normal derivatives of these quantities, as in-

dicated above, at the nodes. The square matrices $\underset{\sim}{A}$ and $\underset{\sim}{B}$ are 3n x 3n elements in size and contain the integral coefficients of $\underset{\sim}{u}$ and $\underset{\sim}{\Omega}$ as indicated in equation (8). Similar remarks hold for the n x 3n size matrices $\underset{\sim}{C}$ and $\underset{\sim}{D}$. The column $\underset{\sim}{E}$ contains the 3n values of the last integral in equation (8) as indicated.

The previously outlined solution strategy when referred to equations (11) and (12) above amounts to the following: Discretize the surface S of B into a number m of surface elements and form and store the matrices $\underset{\sim}{F}$ and $\underset{\sim}{G}$. Specify an appropriate combination of elements $\underset{\sim}{\theta}$ and $\underset{\sim}{\theta}'$ at the nodes corresponding to a well-posed heat transfer problem. Perform the indicated matrix multiplications in (11) involving specified quantities and solve the system (11) for the elements of $\underset{\sim}{\theta}$, $\underset{\sim}{\theta}'$ not previously specified. At this point, the boundary set $\underset{\sim}{\theta}$, $\underset{\sim}{\theta}'$ are completely known.[4]

To begin Step (2), form and store the matrices $\underset{\sim}{A}$, $\underset{\sim}{B}$, $\underset{\sim}{C}$, $\underset{\sim}{D}$, $\underset{\sim}{E}$. Specify the elements $\underset{\sim}{T}$ and $\underset{\sim}{T}'$ which involve the now-known nodal values of the set $\underset{\sim}{\theta}$, $\underset{\sim}{\theta}'$ and also (assumed) known nodal values of the body force potential ψ and its normal derivative ψ'. Next, perform the indicated matrix multiplications to yield a single known vector on the right side of equation (12). Then specify a sufficient number of elements $\underset{\sim}{u}$ and $\underset{\sim}{t}$ corresponding to a well-posed elastostatics problem. Perform the remaining indicated matrix multiplications in (12) involving known or specified quantities at this stage, and solve the system (12) for the remaining unknowns. Now the set $\underset{\sim}{u}$, $\underset{\sim}{t}$ is completely known such that the full complement of surface quantities $\underset{\sim}{u}$, $\underset{\sim}{t}$, $\underset{\sim}{\theta}$, $\underset{\sim}{\theta}'$, $\underset{\sim}{\psi}$, $\underset{\sim}{\psi}'$ pertaining to the desired thermoelastic stress state in B is available at the nodes.

---

[4] If desired, although not necessary for step two in the analysis, we could take $p \in B$ in formula (7) and generate the temperature θ at any desired interior p.

Putting $p \in B \neq P_\eta$ in formula (8) now would yield $u_i(p)$ at any desired p. $\sigma_{ij}(p)$ would be obtained similarly by first obtaining $u_{i,j}(p)$ from formula (8) as previously indicated and then using Hooke's Law (4). Boundary σ_{ij} are obtainable in terms of $\underset{\sim}{\theta}$, $\underset{\sim}{u}$, $\underset{\sim}{t}$ as indicated earlier.

For $B \in E^2$, i.e. a plane problem, S is a curve or the union of several curves, and most of the preceding remarks apply intact with the appropriate reduction in dimension. Note that S_σ is now an element of boundary curve with nodes at each end and one (usually midway) between. There are now three shape functions $M^\alpha(\xi)$, $\alpha = 1,2,3$, which have the form shown in the Appendix, and ξ is a single scalar variable. Matrices which were formerly 3n or 3n x 3n in size are now 2n or 2n x 2n, respectively.

Having outlined the solution process for thermoelastic boundary value problems via the BIE method above in some detail, it is apparent that success with the method depends, in large part, on being able to obtain sufficiently accurate values for the elements of the matrices $\underset{\sim}{A}$, $\underset{\sim}{B}$, $\underset{\sim}{C}$, $\underset{\sim}{D}$, $\underset{\sim}{E}$, $\underset{\sim}{F}$, $\underset{\sim}{G}$. Examination of equations (7) and (8) reveals that the mentioned matrix elements are sums of integrals of the form

$$I^\alpha_{\eta\sigma} \equiv \int_{S_\sigma} M^\alpha(\xi)\Gamma(P_\eta, Q(\xi))J(\xi)d\xi \qquad (13)$$

in which S_σ is a square or equilateral triangle as shown in Figure 5(b) (or the interval -1 to 1 of the straight line for $B \in E^2$), since a mapping to those shapes is inherent in the change of variables implied by the introduction of the shape functions (5). Γ is any of the tensor, vector, or scalar kernel functions indicated in equations (7) and (8). The quantities $c(P_\eta)$, $c_{ij}(P_\eta)$ in equations (7) and (8) respectively prove also to be the sum of certain integrals of the type (13) (see [5], Eqs. (14) and (15) for details). Thus, it is necessary to obtain a sufficiently accurate value for all $I^\alpha_{\eta\sigma}$ by some

numerical integration scheme. For a given choice of surface discretization (number m and arrangement of surface elements and number of nodes n), the manner of obtaining values for $I^{\alpha}_{\eta\sigma}$ is perhaps the most important issue in the solution process. Total computer (CPU) time for a given problem is largely a function of how this is done.

To expand on this matter for $B \in E^3$, note first that two distinct cases in the evaluation of $I^{\alpha}_{\eta\sigma}$ arise: (a) $P_\eta \notin S_\sigma$, and (b) $P_\eta \in S_\sigma$. In case (b), note that since certain of the kernel functions are $O(1/r^2)$ and others at least $O(1/r)$, the integrands, while integrable, require special attention.

The first case, (a), is more straightforward. For integration over the square we use a Gaussian quadrature formula with weight function 1.0 to obtain

$$I^{\alpha}_{\eta\sigma} = \int_{S_\sigma} F^{\alpha}(P_\eta,\xi)d\xi \doteq \sum_{\mu=1}^{\lambda_1}\sum_{\nu=1}^{\lambda_2} A_\mu^{(\lambda_1)} A_\nu^{(\lambda_2)} F^{\alpha}(P_\eta,\xi^{(\lambda_1)}\xi^{(\lambda_2)}) \quad (14)$$

where

$$F^{\alpha}(P_\eta,\xi) \equiv M^{\alpha}(\xi)\Gamma(P_\eta,Q(\xi))J(\xi) \quad (15)$$

and $A_\mu^{(\lambda_1)}$, $A_\nu^{(\lambda_2)}$ are weight factors corresponding to the order λ_1, λ_2 chosen for the quadrature formula [10]. For integration over the triangle we use a special triangularly symmetric quadrature rule by Lyness [11], which symbolically may be written in the same form as (14). In either case, accuracy is in principle a function of the order (size of λ_1, λ_2) of the quadrature rule but so also is the cost (CPU time), so that proper choice of the pair λ_1, λ_2 is an important practical issue for a given integration. After considerable study and experimentation (details will be available in [12]) we have automated the choice of λ_1, λ_2 as a function primarily of the ratio of the distance of the point P_η to some characteristic size of the element S_σ. Secondarily, we increase the order λ_1, λ_2 for a relatively "distorted" element over

and above the order otherwise called for by the "distance" criterion. Both criteria are an attempt to choose λ_1, λ_2 just large enough for a given integrand to give values of integrals, via formula (14), with consistent error.

For case (b), where $P_\eta \in S_\sigma$, we first take account of the fact that $c(P_\eta)$ and $c_{ij}(P_\eta)$ are calculated in a manner (cf. [5], Eqs. (14) and (15)) which analytically requires, for Γ of $O(1/r^2)$, that we evaluate

$$\hat{I}^{\alpha}_{\eta\sigma} \equiv \int_{S_\sigma} (M^{\alpha}(\xi)-\delta_{\alpha\eta})\Gamma(P_\eta,\xi)J(\xi)d\xi \qquad (16)$$

with $\delta_{\alpha\eta} = 1$ whenever node $\alpha \equiv P_\eta$; otherwise, $\delta_{\alpha\eta} = 0$. Thus, if we imagine a local polar coordinate system ρ,ϕ as shown in Figure (6) for typical locations of P_η, we note that $M^{\alpha}(\xi)$ is $O(\rho)$ for $\alpha \neq P_\eta$ and that $(M^{\alpha}(\xi)-1)$ is of the same order for $\alpha = P_\eta$. Thus since $\Gamma(P_\eta,\xi)$ is $O(1/\rho^2)$ and $d\xi$ becomes $\rho d\rho d\phi$, the integrand in (16) is no longer improper and may be evaluated using the same types of quadrature rules previously indicated.

In case (b), since P_η occupies one of the nodes, the "distance" criteria for choice of λ_1, λ_2 no longer has meaning and a threshold choice is made according to a preselected accuracy requirement. Finally, as with the $P_\eta \notin S_\sigma$ case, we can increase the order λ_1, λ_2 for a relatively "distorted" element if necessary.

For $B \in E^2$, for $P_\eta \notin S_\sigma$, a one-dimensional version of formula (14) is used. Here, the choice of order of integration (size of λ) as a function of the proximity of P_η to S_σ is less critical than in three dimensions because of the comparatively fewer total integrations to be done. Hence, we presently pick a threshold size for λ (probably too high for most integrations) and compute all $P_\eta \notin S_\sigma$ integrals for constant λ. Efficiency measures, nevertheless, could be introduced as for three dimensions. Regarding the $P_\eta \in S_\sigma$ case, note that $M^{\alpha}(\xi) - \delta_{\alpha\eta}$ is $O(\xi)$ and since the kernel functions are at

most $O(1/\xi)$ no transformation comparable to the polar coordinate transformation is necessary in two dimensions. There is the problem, however, of one integrand of $O(\log \xi)$ which can be integrated easily enough using a "log" weighted Gauss or by removing the singularity (cf. [7], [13], [14]).

Based on the foregoing discussion, numerical values of all elements of the coefficient matrices $\underset{\sim}{A}$, $\underset{\sim}{B}$, etc. can be calculated automatically by a digital computer upon specifying the cartesian coordinates of all the nodes on the surface S of a body under investigation, the material parameters, and the quadrature parameters λ_1, λ_2.

All subsequent computations were performed on an IBM 370-165 digital computer using single-precision arithmetic. The program and all data for a given problem (Step (1) or (2)) were retained in core. Note that only the matrix of coefficients of unknowns at the nodes need be formed and stored in a square array. The other elements of matrices of coefficients may be immediately multiplied by other quantities as they are generated and stored in column vectors. Individual coefficient arrays need not be formed and stored separately as implied earlier.

2.4 FOUR COMPUTER PROGRAMS

Based on the formulation in Section 2.2 using the discretization/numerical procedures of Section 2.3, four separate computer programs have been created. Two of the programs perform heat transfer analyses (Step 1) for problems in two and three spatial dimensions, respectively. The remaining two programs similarly perform thermoelastic analyses (Step 2). These four programs form the working tools for the research to be described, and they have been developed, checked and exercised in various stages (cf. [1,2,3]) throughout the course of AFOSR sponsorship of the present project.

3. THE PRIMARY RESEARCH PROBLEM DEFINED

3.1 THE BLADE ENVIRONMENT

When in service, the outer surface of a typical turbine blade (see Figure 1) is in contact with hot combustion gases with nominal temperatures of the order 2400°F. As indicated in Figures 2 and 3, the blade has hollow chambers through which cooling air, at a nominal temperature of 1400°F, is pumped under pressure and spewed out through the cooling ("gill") holes and vent holes (cf. Figures 1 through 4). One effect of this air flow through the hollow blade interior is to lower the average blade temperature. Further, a cooling film of air is provided over the blade surface in the vicinity of the gill holes. This is of particular importance at the leading edge of the blade where temperatures are highest. The flow of air and hot gases and the centrifugal field provide the thermomechanical environment for the blade material. All flows and fields are assumed steady in the present analysis.

Clearly, from the above description, stress is induced in the blade material as a consequence of (a) the nonuniform temperature distribution from place to place in the blade, (b) the centrifugal field on the blade, and (c) the gas (and air) pressure and drag acting as surface loads or tractions on the blade. Each of these causes of stress may be regarded separately and the effects superposed. However, according to engineering analysts at General Electric, cause of stress (c) leads to significant values only near the throat (lower portions) of the blade and such values are known to be only a fraction of that expected due to cause of stress (b). Cause of stress (a), the nonuniformity of the temperature field is the least understood and forms the thrust of the present research.

The thermal stress problem is especially interesting due to stress

raising character of the gill holes. These holes contribute to elevated stress in the vicinity potentially in two ways: (i) the nominal thermal stress field due to the gross blade temperature distribution is concentrated near the hole surfaces due to the very geometrical presence of the holes, and (ii) the holes provide for localized additional variation of temperature due to cooling effect of the air carried by the holes. As will be shown, the geometry effect (i) is far more important than (ii). Therefore for purposes of the present research we consider first a fixed blade subjected to zero traction and body force but subjected to a nonuniform temperature field to be described in some detail. Later we superpose, in appropriate fashion, the effect due to the steady centrifugal field.

3.2 THE PRIMARY RESEARCH PROBLEM MODEL

We are most interested in the stress in the immediate vicinity of a single, typical gill hole. Our first model for the "vicinity" of such a hole for a blade with a cross-section of the type in Figure 2 is as shown in Figure 4. This is a thick irregular platelike body obtained by "cutting" along the dotted lines of Figures 2 and 1. This body is bounded as indicated in Figure 4 by portions of the circular "vertical" cooling chamber surfaces, the three "vertical" cut surfaces, the "front vertical" surface, the "top horizontal" cut surface located midway between two typical gill holes, the "bottom horizontal" cut surface through a typical gill hole, and finally by the "half" gill hole surface itself. The angle of inclination α of the gill hole with the front surface is variable but for the specific body of Figure 4 and our subsequent analysis of that particular body, $\alpha = 60°$.

Of special interest now in the body of Figure 4 is the distribution of

normal stress along the edge AB of the gill hole. Of particular interest is the peak stress which occurs, as might be expected, at the "feather edge" of the hole, point A.

To solve for the stress(es) of interest via the analysis method outlined in Section 2, it is necessary to first solve the heat conduction problem for the boundary of the body. This requires a proper statement of well-posed thermal boundary conditions on each surface of the body of Figure 4. Following completion of this first step, θ and θ' (cf. Section 2.2) will be known everywhere on all surfaces S. The second step which uses as input the now known pair (θ,θ') on S, requires a proper statement of well-posed mechanical boundary conditions on each of the surfaces. Output from the second step will include stresses along the edge AB and in particular at point A.

Clearly, the analysis as outlined for the body of Figure 4 depends heavily on a proper statement of the thermal and mechanical boundary conditions on each surface. Hence the rationale for these boundary conditions which in turn leads to the consideration of other problem models will now be considered in some detail.

3.3 BOUNDARY CONDITIONS

The blade portion of the body in Figure 1 is not quite prismatic but it is nearly so and the assumption of identically shaped cross-sections taken normal to the "vertical" or z direction over a blade with indefinite length (z direction) is convenient and easily justifiable for present purposes. Moreover, thermal conditions are assumed to be periodic functions of z with a period of one gill hole spacing such that the fields of interest, e.g. stress, displacement, are also similarly periodic[5]. The described periodicity

[5] The centrifugal field is assumed zero et. seq. until stated otherwise.

or "cyclic symmetry" clearly demands the following: (a) the heat flux θ' is zero on the horizontal cut surfaces of Figure 4, (b) each of these surfaces must remain plane under thermal load, and (c) the shear traction must be zero on each of these surfaces.

Now from typical thermal data supplied by General Electric, it is possible to supply a non-zero value of θ' over the vertical cut surfaces of Figure 4. Unfortunately, the variation of such θ' with z, while probably not great over the period, is unknown and we thus assume, in the absence of better information, θ' to be independent of z on the mentioned surfaces. For the remaining surfaces, i.e. the vertical part-cylindrical chambers, the gill half-hole surface, and the front, gas/gas-air mix, contacting surface, typical data for k, h_c and θ_o in a convective boundary condition of the type

$$(k/h_c)\theta' = (\theta_o - \theta) \tag{17}$$

were made available by General Electric. In Equation (17), k is the thermal-conductivity, h_c is a convective surface heat transfer coefficient and θ_o is a "contact-fluid" temperature. Numerical values for h_c and θ_o over the relevant surfaces were made available such that with the mentioned known values of θ' on the cut surfaces, it is possible to pose and solve a heat transfer problem for the body of Figure 4. Again, h_c and θ_o are taken independent of z. Nevertheless, the presence of the gill holes yields θ and θ' which depend on z over the gas or air contacting surfaces as required.

With the thermal boundary data in hand it remains to consider the mechanical boundary conditions on the surfaces of Figure 4. Now as mentioned earlier we may assume the gas or air contacting surfaces to be traction free. Thus the gill half-hole surface, the vertical part-cylind-

rical surfaces and the front surface have the simple condition $\underset{\sim}{t} = \underset{\sim}{0}$. On the lower cut horizontal surface we may state the symmetry condition as $t_s = 0$ and $u_n = 0$ where s and n refer to in plane and normal directions, respectively. On the upper cut horizontal surface, the condition that it remain plane and shear traction free is helpful but not as immediately complete as the lower surface condition since the location of the plane remains unknown. We will return to this boundary condition shortly.

The vertical cut surfaces of Figure 4 present the most interesting consideration of boundary conditions. The tractions on these surfaces clearly arise from the surrounding portions of the blade from which the piece is cut. These tractions are non-zero to the extent that the thermal field in the whole blade is non-linear in the cartesian coordinates. Thus to obtain representative values for the tractions $\underset{\sim}{t}$ on these vertical cut surfaces it is necessary to consider gross blade behavior. We accomplish this in the following way.

The thermal conditions as already noted are periodic in the variable z, and under the prismatic assumptions, this periodic variability is strictly a consequence of the presence of the gill holes. In their absence the thermal field would be plane or independent of z. The question arises then to what extent do the gill holes alter the thermal tractions which would exist on the vertical cut surfaces of Figure 4 in the absence of gill holes assuming, of course, comparable overall temperature distributions in the blade in the two cases? This question is sensibly addressed as follows. Examine the cross-section of Figure 2. Ignore the geometrical influence of the periodically arranged gill holes and perform a heat transfer (Step 1) and a subsequent thermoelastic analysis (Step 2) on the cross-section of the blade shown bounded externally by the airfoil shape and internally by the circular

boundaries. For this plane (strain) analysis use actual thermal boundary conditions for that portion of the blade in Figure 2 shown in Figure 7. Typical numerical data for the boundary conditions are available from the manufacturer. Use also the (in-plane) zero traction condition and calculate the tractions on the three dotted lines of Figure 2, which are the edges of the three vertical cut surfaces of Figure 4. These computed thermal tractions are clearly an approximation, nevertheless an excellent approximation we think, to the actual tractions existing on the vertical cut surfaces of Figure 4. The difference between these two sets of tractions would be due to the influence of the cooling holes on the gross thermomechanical behavior of the blade which gave rise to the computed tractions in the manner just indicated. We argue that the difference would be slight especially on the plane midway between gill holes and the tractions computed as indicated represent an excellent approximation to the "true" tractions. The latter would be clearly unavailable without an incredibly complicated three dimensional analysis of a body with the same cross-section as in Figure 2 but at least several gill holes thick in which the holes, despite their small size and probable influence on the variables at present issue, would have to be modelled.

On the assumption that the tractions computed via the above described planar analysis represent a valid set to be placed on the vertical cut surfaces of Figure 4, it now remains to precisely state a boundary condition for the top cut horizontal surface argued earlier to remain plane and shear traction free.

Toward this end note first that the magnitude of normal traction $t_n \equiv t_z$ ($t_s = 0$) acting in the out-of- plane z direction, under the plane strain assumptions for the plane thermoelastic solution for the cross-section

of Figure 7, is given by

$$t_z = \nu(\sigma_{xx} + \sigma_{yy}) - \alpha E\theta \tag{18}$$

wherein σ_{xx} and σ_{yy} are the in-plane normal stresses available from the mentioned plane strain solution. Numerical values of t_z are thus available, in practice, at a selected array of points on the material occupied area A of Figure 7.

*We may now imagine a prismatic body of indefinite length with the cross-*section of Figure 7 (no gill holes) under the plane $\theta(x,y)$ distribution, and traction free on its lateral surfaces. On any cross-section (i.e. Figure 7) t_z acts and the deformation in the body is plane. If we now calculate the resultant axial force F on this body and the components of resultant couple according to

$$F = \int_A t_z dA, \qquad C_x = \int_A t_z y dA, \qquad C_y = -\int_A t_z x dA \tag{19}$$

and define tractions t_o and t_1 respectively given by

$$t_o = -F/A \tag{20}$$

$$t_1 = \frac{(xI_{xx} - yI_{xy})C_y + (xI_{xy} - yI_{yy})C_x}{I_{xx}I_{yy} - I_{xy}^2} \tag{21}$$

we may superpose to yield a resultant traction.

$$t^* = t_o + t_1 + t_z \tag{22}$$

In the above, xy are coordinates relative to the centroid of the cross-section of Figure 7, and I_{xx}, I_{yy}, I_{xy} are the area moments and product of inertia of A relative to the xy coordinates. Clearly, the net force and couple

associated with t^* are zero. Further, the prismatic body subjected to $\theta(x,y)$ and t^* only is a representative model[6] of a typical length of the blade in a static thermoelastic state ignoring end effects, the gill holes, and, of course, the centrifugal field.

It is a relatively straightforward analytical exercise to now calculate the displacement of one cross-section relative to another due to the $t_o + t_1$ distribution acting on this bar. In particular we can find the displacement of one cross-section one-half gill hole spacing away from another. Such a cross-section, like all others, remains plane under $t_o + t_1$ load. The position of this plane, as well as others, is clearly a function of the gross temperature field in the blade uninfluenced to any significant effect by the actual presence of the gill holes which occupy only an insignificant portion of the volume of the blade material. Note that conditions of symmetry demand that even in the presence of gill holes, cross-sections through gill holes must remain plane. Clearly these planes, with or without gill holes, are almost identical. Thus we now have our boundary condition for the top surface of the body of Figure 4, namely, a normal displacement $u_n \neq 0$ which is identical with the mentioned analytically determined displacement arising from the tractions t_o and t_1.

Note that knowledge of the non-zero displacement u_n, computed as described, on the top surface of Figure 4 is a more meaningful boundary condition than a prescription of t^*. This is of the utmost significance in the present analysis and is true for the following reason. While the t^* actually present over the small part of the cross-section (top surface of Fig. 4) may be significantly different than that given by Equation (22), i.e. locally altered by the presence of the gill

[6] Note that Figure 7 depicts an incomplete blade cross-section. The "tail" portion is missing. A brief discussion of the effect of this on the analysis is given on page 27 paragraph 2.

hole, u_n is computed from t_0 and t_1 which in turn are based on the distribution of t_z over the entire area of Figure 7. Thus the u_n used is substantially the same with or without gill holes.

We now have a complete set of well-posed mechanical boundary conditions for the thermoelastic body of Figure 4. Numerical results and further discussion of this "Primary Research Problem Model" are given in Section 4.

3.4 THE EFFECT OF THE CENTRIFUGAL FIELD

By comparison to the above consideration of boundary conditions, the boundary conditions on the body of Figure 4 to take account of the centrifugal field of the blade are fairly simple. Using the condition $u_n = 0$, $t_s = 0$ on the lower horizontal cut surface, $t_n = \sigma_o$, $t_s = 0$ on the upper horizontal cut surface, with all other surfaces traction free, is reasonable and consistent with the manufacturer's practice. Isothermal conditions are assumed and the presence of centrifugal "body" force over the small volume itself may be sensibly neglected by comparison to σ_o which approximates the centrifugal pull of the adjacent portion of the blade across the surface on which σ_o acts. Again the distribution of normal stress along the edge AB of the gill hole is the desired output from the solution of this problem.

Note that the condition $u_n = 0$ on the lower horizontal surface of Figure 4 assumes that this surface is a plane of symmetry for the body plus its reflection in that surface. This body according to the preceding statements is loaded in simple uniform tension on its upper and lower surfaces. How well this approximates the actual state of stress due to the centrifugal field is somewhat a function of the gill hole spacing vs. gill hole diameter. Indeed, if the gill holes are sufficiently far apart the assumption of uni-

form σ_o midway between holes is a good one. However, in the extreme, where the holes are very close together, e.g. less than one hole diameter apart, the above assumption is probably poor. In the latter case a better approximation would be to first recognize that the surfaces between holes while not plane are similarly deformed under centrifugal loading and it is perhaps not too gross an assumption to take the portions of the surfaces involved, i.e. the top surface of Figure 4, its mirror image, and therefore also the bottom horizontal surface of Figure 4 to be parallel planes. Thus, an alternative boundary condition for the body of Figure 4 to simulate centrifugal loading would be $u_n = 0$, $t_s = 0$ on the lower surface, $u_n = u_o$, $t_s = 0$ on the upper surface.

Numerical data for unit input values of σ_o and u_o, thereby using both assumptions, are given and compared in Section 4.

4. SOLVED PROBLEMS FOR THE PRIMARY MODEL

4.1 THE PLANE PROBLEMS FOR FIGURE 2

According to the discussion of boundary conditions in Section 3.3 it is necessary to first solve the heat conduction problem for the blade cross-section of Figure 7. Values of h_c and θ_o were given by G.E. on a scale drawing from which we were able to state a thermal boundary condition of the type (17) for each part of the boundary shown in Figure 7. Note that the gill hole, being below or above the cross-section of Figure 7, is not part of the boundary for this analysis which is planar. Using the discretization depicted in Figure 7 with m = 67 line segments and n = 134 nodes, our heat conduction analysis yielded, for the specific boundary data used, the isotherms shown in the figure. The depicted temperature distribution compares favorably with the manufacturer's temperatures obtained by other means.

Next, assuming in-plane tractions on the body of Figure 7 to be zero, we calculate, through Step (2) of the analysis, the stress distributions across the three surfaces, i.e. the three dotted lines in Figure 7. Results and material properties are shown in Figure 8. Distribution of normal stress is shown in detail. Directions of shear stresses, which are an order of magnitude smaller than the normal stresses, are indicated by a single arrow as shown. Thus, the major effect of the thermal field in the blade cross-section is to produce bending, via the three "thermal couples" shown in Figure 8 on the piece of the blade indicated. While we have only sketchy stress data from the manufacturer with which to compare, our results are believable when compared with the essential features of thermal stress in a hollow cylinder, cool on the interior and hot on the exterior. This problem was treated in some detail in [2,5]. Additional discussion of the cylinder problem, and how a major stress inducing consequence of the temperature distribution in the

blade material is present in the cylinder problem will be given subsequently.

The distribution of stress shown in Figure 8, assumed to be uniform over the length of the vertical cut surfaces of Figure 2, represents the needed tractions on the mentioned surfaces, as discussed in Section 3.3. These tractions represent the major mechanical influence of the surrounding blade material on the "piece" in Figure 2 as required. The remaining influence, i.e. the traction t_z is readily obtained. A plot of the t_z distribution is shown in Figure 9. Approximately 245 points were positioned over the area A of Figure 2 at which σ_{xx}, σ_{yy}, and θ were obtained from which t_z was computed via Equation (18). From this t_z distribution, F, C_x, and C_y from Equation (19) were obtained. Based on a nominal constant reference temperature of 1800°F, the computed t_z distribution yielded the following values

$$F = -498.60 \text{ lb}, \qquad C_x = 3.03 \text{ in-lb}, \qquad C_y = -45.19 \text{ in-lb} \tag{23}$$

Therefore $t_o = 9{,}082 \text{ lb/in}^2$ from Equation (20). Further, $A = .055 \text{ in}^2$, $I_{xx} = 2.77 \times 10^{-4} \text{ in}^4$, $I_{yy} = 7.96 \times 10^{-4} \text{ in}^4$, $I_{xy} = 0.11 \times 10^{-4} \text{ in}^4$. From these numerical data the linear t_1 distribution is now known via Equation (21). Thus the plane displacement $u_n \equiv u_{no} + u_{n1}$ of any cross-section of the type in Figure 7 relative to any other is now obtainable as the simple deformation due to the tractions $t_o + t_1$. In particular the displacement u_n of the "top" surface of Figure 4 relative to the "bottom" surface is available and could be used, as indicated in Section 3.3 as our "top" surface boundary condition.

However, top surface boundary condition may be simplified further by noting that the actual values of F, C_x, and C_y listed above are somewhat arbitrary. Specifically, it is clear that any change in the arbitrarily chosen reference temperature of 1800°F would lead to a proportional change in t_o or F. However, the corresponding constant part of the displacement u_n,

i.e. u_{no}, would be similarly changed and the arbitrariness compensated in the superposition process. Similar remarks apply for t_1, C_x, C_y, and the linear part of the displacement u_n, i.e. u_{n1}, since, in principle, an arbitrary non-constant but linearly varying reference temperature distribution could have been chosen. Indeed, there exists a (apriori unknown) linear reference temperature distribution for which F, C_x, and C_y would all be zero. For this (non-arbitrary) reference distribution, the condition $u_n = 0$ on the "top" surface of Figure 4 would be the proper boundary condition. This linear reference distribution may now be obtained as follows. Note first that

$$u_{no} \equiv \frac{t_o}{E} \ell = 1.12 \times 10^{-5} \text{ in.} \tag{24}$$

wherein $t_o = 9{,}082$ lb/in^2, $E = 24.3 \times 10^6$ lb/in^2, and $\ell = 0.03$ in is one-half the gill hole spacing in the present design configuration. Secondly, since I_{xy} is an order of magnitude smaller than I_{xx} and I_{yy} and since C_x is similarly small compared to C_y, the bending implied by Equation (21) is nearly symmetrical (i.e. the neutral surface of bending is inclined only 8.8° from the y axis (Figure 7)). Thus with negligible error for present purposes t_1 is approximately given by

$$t_1 \doteq \frac{C_y x}{I_{yy}} = -5.68 \times 10^4 \times \text{lb/in}^2 \tag{25}$$

wherein $C_y = -45.19$ lb-in and $I_{yy} = 7.96 \times 10^{-4}$ in^4. Therefore, u_{n1} has the form

$$u_{n1} = \frac{t_1 \ell}{E} = \frac{C_y \ell}{E I_{yy}} x = -7.01 \times 10^{-5} \times \text{in.} \tag{26}$$

Now the desired reference temperature distribution has the form

$$\theta_R = a + bx + cy \tag{27}$$

where a, b, and c are constants. Since the unknown u_n has the form

$$u_n = \alpha(a + bx + cy)\ell = (1.12 - 7.01x) \times 10^{-5} \text{ in.} \qquad (28)$$

in which $\alpha = 9.2 \times 10^{-6}/°F$ is the coefficient of thermal expansion, it is clear that the choices

$$a = 40.6°F + 1800°F, \qquad b = -254.0°F/in, \qquad c = 0 \qquad (29)$$

gives the explicit form for the reference distribution. Subsequent analyses for the primary research problem model of Figure 4, based on this particular θ_R as the reference temperature distribution may use the simple top surface boundary condition $u_n = 0$. All arbitrariness with regard to reference temperatures in subsequent calculations has thereby been removed.

There is one remaining difficulty with the modelling and superposition solution process under the present circumstances. Unfortunately, no thermal or other data compatible with the data for the portion of the blade cross-section shown in Figure 7 were available for the "tail" portion not shown. To have made a more representative model, t_0 and t_1 should be computed on the basis of F, C_x, and C_y (obtained from t_z) for the entire cross-section. However, modification of our present analysis, should data for the tail portion of the blade become available, is readily made. A new, perhaps more representative, value for u_n could easily be computed analytically leading to a (possibly) new reference temperature distribution. We suspect alterations in the following results would be slight.

Having obtained all the necessary data from the above described plane analysis, we proceed now to the three-dimensional analysis for the primary model (cf. Figure 4, discussion in Section 3.3).

4.2 HEAT CONDUCTION ANALYSIS

Figure 10 depicts the primary research problem model (cf. Figure 4) with

dimensions to scale and a partial view of the discretization pattern (ref. Sec. 2.3) used for this part of the analysis. The number of surface elements $m = 69$ and the number of nodes $n = 215$. The circular cooling chambers have diameters of 60.0 mils and 140.0 mils, respectively, the gill hole diameter is 16.5 mils, and the length ℓ (z direction) of the piece is 30.0 mils, i.e., one-half the gill hole spacing for this particular configuration. These dimensions and discretization pattern are used for all subsequent thermoelastic analyses of the primary research problem model.

As discussed in the second paragraph of Section 3.3 we now input the data supplied by G.E. to Equation (17) for each of the fluid contacting surfaces. Part of these data were applicable to the previously performed planar analysis for the cross-section of Figure 7, but now we have the gill hole and the length ℓ to contend with and thus, of course, a three-dimensional problem. Despite the presently necessary assumptions about θ' not varying with z, and similar assumptions on h_c and θ_o in Equation (17) (ref. parag. 2 Sect. 3.3), a heat conduction analysis for the body of Figure 10 under the stated boundary conditions leads to a smooth and believable <u>three-dimensional</u> variation of temperature over the body. Since the subsequently relevant outcome of this heat conduction analysis, i.e. θ and θ' at all the nodes on the surface of the body are not of intrinsic interest, and difficult to display meaningfully, these data are not shown. No data from General Electric with which to compare any of our three-dimensional temperature variations were available, of course, which is consistent with z varying input data being unavailable from G.E. as previously mentioned. Nevertheless, our solution in its x,y variation is consistent with their data and our own plane solution previously described. Further, the local thermal effect of the gill hole manifests itself realistically by cooling the piece of Figure 10 by amounts and in places that are con-

sistent with reasonable expectations. Step (1) for the research problem model is now completed.

4.3 THE FULL THERMOELASTIC PROBLEM

With the complete set (θ,θ') known numerically at all the nodes for the body of Figure 10, we begin Step (2) by supplying the mechanical boundary conditions as follows. The tractions of Figure 8, assumed constant (with respect to z) over the "vertical" cut surfaces of Figure 10, are input as numerical values of normal and shear traction at appropriate nodes. Values of traction at nodes on all fluid contacting surfaces are zero. Following the adjustment in (θ,θ') to provide the specific reference temperature distribution θ_R (ref. Eqs. (27) - (29)), we use the condition $u_n = 0$, $t_s = 0$ at all nodes on the "top" horizontal surface. This condition is now identical with that on the "bottom" surface of Figure 10.

Our thermoelastic solution based on the stated boundary condition yields the thermoelastic stress field throughout the body of Figure 10. Of primary interest is the normal stress distribution on the bottom surface, (cf. Figure 4) along the line AB, i.e. one edge of the hole. Point A is of special interest, i.e. the "feather edge". The stress distribution along this line and along the "front edge" AC are shown in Figure 11. Further, the "hoop stress" distribution, i.e. the stress at the surface of the hole in directions tangent to the hole, is shown in Figure 12.

The stress at point A as shown is tensile, and our analysis predicts, as probably expected, a high gradient of stress as point A is approached along lines AB and AC. Compression is indicated along most of the length AC whereas tension is indicated along the entire length AB[7]. Higher levels of tensile

[7] These results disagree with data reported for a related problem in [3], Figure 7. An error was discovered which invalidates that data in [3].

stress at the inside (point B) end of the gill hole are indicated than at the feather edge (point A). Further, the magnitude of compressive stress at C is comparable to that of the tensile stress at A. These results require some interpretation and discussion.

As an aid to interpretation of our numerical data, to help assess their reliability, and to gain greater insight into the mechanism for the inducement of stress in the body of Figure 10, we imagine the following separate problems which, when "added together", yield the stress results depicted in Figures 11 and 12.

Consider the body of Figure 10 at uniform temperature but loaded on its "vertical" cut surfaces with the tractions of Figure 8. The top is traction free (unconstrained), and the bottom (et. seq.) is held plane by normal tractions only, which, as before, are the quantities of interest. This problem, as far as the body of interest is concerned, is isothermal, but the load is a set of tractions which arise from the fact that the body is part of and, of course, acted upon by the surrounding blade - the whole being in a thermal environment. Stress distributions along lines AB and AC for this problem (called component problem (i), et. seq.) are shown in Figure 13, and the hoop stress distribution is shown in Figure 14.

The peak tensile stress at point A for this loading is about twice the value shown in Figure 11. The way the tractions are applied (cf. Figure 8) clearly is consistent with high tensile stress at A and, less intuitively perhaps, consistent with the hoop stress pattern. This means, of course, that the other "components" of this problem, namely, (ii) the actual $\theta \neq 0$ distribution over the body of Figure 10, and/or (iii) the constraint condition $u_n = 0$ at the top surface provide sufficient compression to reduce the tensile stress at point A by 50% and otherwise yield the dominant compression along most of

line AC, as shown in Figure 11. Further, these other "components" must be responsible for the high tension along the line AB.

To assess the separate roles of components (ii) and (iii), we consider the body of Figure 10 with no applied tractions whatsoever except for the bottom which has the same boundary condition as before. Here we put in the $\theta \neq 0$ distribution (referred to θ_R) and thus solve the component problem (ii) to assess the influence of the (non-linear) temperature distribution on the piece of Figure 10, removing the constraining influence of the surrounding material. Here, we find that the levels of stress along lines AB, AC, and the hoop stress distribution are comparatively insignificant. Our solution of this problem yields nominal (compressive) stresses of the order two to three thousand pounds per square inch along line AC, for example, with an increase to about ten thousand right at point A. The stress level along line AB is similarly low. Thus it seems clear that the constraint or mechanical effect (albeit arising from thermal conditions in the overall blade) of the blade material on the piece of Figure 10 dominates in producing the stresses of interest. That is, component problems (i) and (iii) dominate. More specifically, the lateral tractions of Figure 8 lead to high tensile stress at the feather edge (point A), which is reduced by the compression induced by the constraint ($u_n = 0$) on the top surface of Figure 10, and, to a lesser extent, by the $\theta \neq 0$ distribution on the body itself. Further discussion of this and related matters, and the assumptions on which the various described problems are based will be made subsequently.

4.4 STRESS DUE TO THE CENTRIFUGAL FIELD

As mentioned in Section 3.4, we consider two models, i.e. two problems, each with a different top surface (Figure 10) boundary condition, to represent the centrifugal field.

The first model assumes $t_n = \sigma_o = 1$ on the top surface of Figure 10 to simulate the centrifugal field. With this model and the previously used discretization pattern, our isothermal elastic analysis yields the stress distributions along the edge of the gill hole AB and the front edge AC as shown in Figure 15. The maximum tensile stress as shown in Figure 15 yields a stress concentration $\sigma_{max}/\sigma_o = 9.4$. This figure is in satisfactory agreement with the stress concentration of 8 for the related problem of a flat plate with a 60° inclined hole in tension (discussed at length in [2]), considering, of course, the more irregular shape of our body.

The second model assumes $u_n = u_o = 1$ on the top surface of Figure 10 to simulate the centrifugal field. As noted in Section 3.4, this boundary condition is probably better than the uniform σ_o for closely spaced gill holes. The present spacing of 60 mils is typical, although we understand there exist configurations of from considerably less than 60 mils spacing up to 120 mils or greater for a gill hole diameter of 16.5 mils. Really, any spacing/diameter ratio could be expected, and the two types of boundary conditions used above probably provide upper and lower bounds on the centrifugally induced stress-concentration for the presently used ratio of hole spacing to diameter. The same is likely true for any other ratio.

Once again our isothermal elastic analysis yields the "edge AB" and "edge AC" distributions as shown in Figure 16. Here the displacement $u_o = 1$ is statically equivalent to an average applied tensile traction σ_{avg}. Based on σ_{avg}, a stress concentration at the feather edge of the hole (point A, Figure 16) is $\sigma_{max}/\sigma_{avg} = 5.7$. This figure is considerably lower than the 9.4 above, as is to be expected from the inherent difference in the type of input (cf. discussion [2] pg. 19).

5. DISCUSSION

5.1 ADEQUACY OF DISCRETIZATION

The question of integrity of the numerical data presented in the previous sections is largely a function (a) of the adequacy of the discretization used for the various problem models and (b) the significance and reliability of the boundary conditions, symmetry assumptions, etc., and input thermal data. Both of these issues are subject to some reexamination as follows.

The discretizations used for the plane problems are more than adequate to the task at hand. Our experience with such plane discretizations, and the outcome of our experiments in this regard with the present problems, leaves little doubt that the results of our plane analyses are as accurate as the knowledge of input thermal data and stated boundary conditions would justify. The discretizations used for the three-dimensional problems admittedly could be finer, to provide more resolution in the regions of highest stress gradients, for example. However, finer three-dimensional discretizations come only at considerable cost and effort (cf. discussions in [1,2,3]). Moreover, the work [1,2,3] was heavily devoted to assessing the reliability of discretizations comparably fine to those used here in connection with problems for which we could judge accuracy directly. Indeed, those problems were chosen for their essential similarity to the ones at hand. Further, those problems helped to exercise and check all of the important thermal and mechanical loading effects and geometrical features of the solved problems in Section 4. For example, the various isothermal stress-concentration problems solved in [1,2], with comparably fine or cruder discretizations, lend confidence to that part of the stress of interest due to mechanical loading on the "top" surface of Figure 10. Confidence in the temperature distributions and thermally induced stresses is

similarly gained from the work reported in [2]. One "loading feature" in the present analysis, not tested in [1,2], is that of the body of Figure 10 loaded essentially in bending by the "couples" of Figure 8 leading to the results of Figures 13 and 14. Thus, to lend the level of confidence in this part of the analysis that we have in the other parts as a consequence of earlier work, we consider the problem described in the next section.

5.2 PLATE WITH STRAIGHT-THRU-HOLE IN BENDING

Figure 17 shows to scale one quarter of an elastic plate with dimensions 10 x 16 x 4. The radius of the hole is unity, and the discretization pattern used to solve the problem to be posed is as indicated in the figure. We load this plate in simple lateral bending by applying a linearly distributed bending traction, the tensile part of which is as shown in Figure 18. The output for this problem, the stress distribution (tensile part only) along the mid-surface through the hole, is shown in the same figure. The stress concentration, defined as the ratio of the peak stress at the hole to the nominal bending stress from our solution, is 2.49. This compares favorably with an expected value from the literature of 2.62. Thus with the discretization pattern shown, which is comparably fine to that shown in Figure 10 for the research problem, we are able to achieve peak stress accuracy to within 5%.

Of course, the hole of Figure 10 is sharply inclined to the "front" surface, which leads to higher stress gradients and places more demand on the discretization pattern than the straight-thru hole. Nevertheless, judging from the predicted stress concentrations near straight-thru holes under bending and tension, the bending stress concentration is of the same order of magnitude as the tensile one. Thus since we have already (cf. [2]) tested a comparably fine discretization for the inclined hole under tensile load we have reason to believe that peak stress data in Figures 11 through 14 are as accurate as

the data in Figures 15 and 16. Even an accuracy estimate of perhaps 10%, or a more pessimistic estimate of 20% to 25% accuracy, in our judgement, would still render the mentioned data of value in providing insight into the general picture of how stress is induced in the vicinity of the gill holes.

5.3 SIGNIFICANCE OF BOUNDARY CONDITIONS

The question raised earlier of the significance and reliability of the assumptions of cyclic symmetry on the turbine blade, assumed to be prismatic and indefinitely long, and the necessary consequences of plane surfaces should now be reexamined in light of the results for component problems (i), (ii), and (iii) in Section 4.3.

Recall that the problems are (i) the "isothermal" body under the "lateral couples" of Figure 8, (ii) the "free" body subjected to only the $\theta \neq 0$ distribution, and the implied third problem (iii), which is the body of Figure 10 subjected to the top surface condition $u_n = 0$. In the three problems, we submit that the boundary condition $u_n = 0$ on the top surface for problem (iii) is most questionable. This in turn questions the validity of the $u_n = 0$ condition on the full thermoelastic problem as originally posed and, therefore, the validity of the data in Figures 11 and 12.

If the blade were very long (we assumed indefinitely long), the stated boundary condition and thus the numerical data (Figures 11 and 12) would be reasonably representative for gill holes away from the ends. On the other hand, for a gill-hole near the end of the blade, the top surface boundary condition more properly should be $\underset{\sim}{t} = 0$ as was used in component problem (i) (Figures 13 and 14). Thus, ignoring the contribution of component problem (ii), it appears that the tensile stress at the feather edge, point A, lies somewhere between the two extremes. That is the 43,000 figure is probably too high for most gill holes, and the 19,400 figure is probably too low,

especially for the holes nearer the free end. Of course, the lower gill holes are subject to the larger stress-concentration due to the centrifugal field, so there is a compensating effect, i.e. higher tensile stress due to the thermal field where the centrifugal effect is smaller and vice-versa.

It is possible that if a finer picture of the thermal distribution over the surfaces of Figure 10 were available from the manufacturer, especially as regards the variation with depth of the parameters h_o and θ_o, component problem (ii) could have made a more significant contribution to the stress fields of interest. However, our basic finding that the stresses of component problem (i), i.e. the stresses induced by the lateral traction distribution, are most important is consistent with the information available from an idealized but essentially similar problem.

This idealized problem consists of a thick circular cylinder with cool inner surface and hotter outer surface held in a configuration of plane strain. This problem was discussed at length in [2] pg. 9 ff, and, upon reflection, it exhibits many of the important characteristics of the primary research problem. We have two cool inner surfaces (circular cooling chambers) instead of one, but the outer surface is hot in both cases. The transverse stress in both cases (cf. [2], Table I and the present Figure 8) produces bending on a portion of the cylinder as it does on our research body. Moreover, if one considers only a piece of the circular cylinder, e.g. a piece subtending an angle of say $\pi/4$ radians, and subjected to the lateral bending tractions from the rest of the cylinder contacting the piece, the inplane stresses induced by those tractions under isothermal conditions for the $\pi/4$ piece are indistinguishable from those obtained if the actual temperature distribution over the piece is included. This observation lends confidence to our conclusion that component problem (ii) is relatively insignificant. In short, the

transverse stress of Figure 8 acting on the body of Figure 10 is essentially similar to that in the cylinder problem. This is the stress that "is concentrated by" the gill hole and of primary interest. This observation is contrary to our earlier expectations [1,2,3] that perhaps the local θ field on the piece of Figure 10 was at least equally important. Thus, the problem of a circular cylinder, cool inside and hot outside, with a hole drilled from outer to inner surface (at a variable angle to the vertical direction) would be an excellent model for the important phenomena in the gill-hole-cooled turbine blade. This model is especially applicable, we judge, for the blade cross-section of Figure 3. If this is so, the bending problem of the previous section has additional significance in the following sense. Imagine the applied couples to be thermally induced, since the plate is imagined cut from the blade of Figure 3. Then the isothermal analysis, previously argued to be valid for the small piece, yields the stress concentration of about 2.5. Variations on this problem, i.e. a parameter study, could be performed, by varying the angle of inclination of the gill holes and, although less important perhaps, allowing the plate to have some curvature. These problems would clearly simulate the conditions in the vicinity of the gill holes depicted in Figure 3. Such a parameter study could be readily done with our developed computing capability pending the necessary thermal data for specific blade configurations from the blade manufacturer.

A final reference to the cylinder problem is in order. This problem was solved in [2] under plane-strain assumptions. If we imagine a superposed uniform traction t_o, acting on the ends of the cylinder, sufficient to render the cylinder axial-force-free (or equivalently use a proper reference temperature θ_R), we have an essentially similar situation to that of the primary research body of Figure 10. Specifically, a segment of the cylinder is under an axial

traction t^* which is tensile near the inner surface of the cylinder and compressive near the outer surface. This pattern is consistent with the data of Figure 11. Further, Figure 19 depicts the t^* distribution on the top surface of the research body, and it will be noted that it exhibits the same essential character as the cylinder t^* distribution. Note in passing that the t^* distribution of Figure 19 is locally disturbed by the presence of the gill hole, as anticipated in paragraph 3, page 21.

This reference to the cylinder problem clarifies somewhat the difficulty with the top surface boundary condition in the research problem, or, if preferred, the difficulty with the contribution from component problem (iii). If we imagine the blade to be (crudely but essentially) modelled by a hollow unconstrained cylinder of finite length, the top surface boundary condition used in (iii) represents conditiors near the midplane of a long cylinder. Nearer the ends, or if the cylinder is shorter, e.g. only two or three outer diameters long, the top surface condition $u_n = 0$ leads to values of axial tension on the inner surface and compression on the outer surface which are higher than probably realized. It is therefore difficult to judge the validity of the contribution of component problem (iii) for a specific gill hole, depending on its location relative to the ends, i.e. top end and throat, of the blade. Nevertheless, the nature of the contribution of this component to the stress at point A is similar to the contribution of the centrifugal field, whereas the contributions of component problems (i) and (ii) were comparatively little understood.

6. SOME FINAL REMARKS

We think it is appropriate to close this investigation by briefly stating what, in our view, are the more important contributions arising from it and by summarizing what we think to be of questionable validity and why. In addition, a few remarks will be made regarding suggestions for improving reported data through further research.

Within the continuum theory of linear, homogeneous, isotropic, steady-state (classical) thermoelasticity, this research effort has produced four separate computer programs capable of performing reliable numerical analyses for a wide variety of plane and three-dimensional problems governed by the theory. This computing capability is quite contemporary, competitive, and in some cases better, we judge, than alternative numerical methods for problems of thermoelasticity. Indeed, the amount of interest in the BIE method in general, and our specific programs in particular, shown by the academic and industrial communities here and abroad is, perhaps, witness to that fact. The existence, therefore, of the four programs, motivated by and created largely for the solution of the primary research problem, is probably the most important outcome of this investigation.

We should emphasize that these programs may be used effectively for a broad class of problems in elasticity, with or without thermal effects or body force. Clearly the data and problem descriptions for the present work were quite specific. However, the programs may be used for analysis using data for other problem descriptions and thermomechanical configurations, as needed, in whatever discipline classical heat conduction and/or (thermo) elasticity problems occur.

Regarding our "solution" of the primary research problem and the described related problems, we feel that there is sufficient uncertainty that the turbine

blade material is modelled accurately by classical thermoelasticity to relate all of our results to "reality" only with prudent reservation. That point being taken, it is important to recognize that output data is no more reliable than input data and herein is the source of some uncertainty regarding some of our results. Specifically, we were prepared to enter thermal data (e.g. in Eq. (17)) with considerable detail, but the availability of such data from the blade manufacturer was fairly crude. This was less true regarding the x,y variation of such data as input into our plane analyses but sufficiently true for our three-dimensional, non-isothermal analyses to cause concern about the meaning of the output data beyond its being representative, certainly in the "ball park", and reasonably self consistent whenever self consistency checks were available and made. On the other hand, our isothermal solutions, e.g. the centrifugal field results (Figures 15 and 16), we judge to be excellent, granting, of course, whatever uncertainties accrue to the two input load models (boundary conditions) used. Further, component problem (i), leading to the results of Figures 13 and 14, are, we judge, similarly good despite the dependence of the shown results on thermal data. This is true since the thermal data at issue for problem (i) is exclusively plane and given by the manufacturer in probably sufficient detail for the purpose at hand. Added to the thermal data uncertainty for component problems (ii) and (iii), and hence for the full thermoelastic problem (the "sum" of problems (i), (ii), and (iii)), is the uncertainty previously discussed at length regarding the horizontal surface (Figure 10) boundary conditions.

Despite the above-mentioned difficulties with certain of the data, our analysis, broken down as described, gave us, and hopefully will give the reader, valuable insight into the relative roles played by the various components of the thermal field and the centrifugal field in producing stress at the

feather edge of a gill hole.

By way of further research, a renewed attack on the primary research problem model could be profitably undertaken with the availability of more detailed input thermal data. To obtain such data for a more detailed description of the parameters h_c and θ_o would require fluid-flow/heat-transfer research beyond the scope of the present investigation. A perhaps better set of mechanical boundary conditions than those used for Figure 10 could be obtained from a three-dimensional thermoelastic analysis of the entire blade minus, of course, the individual gill holes. Here again, however, the axial variation of temperature would have to be provided from the manufacturer. A fixed throat portion of the blade with the other end free would perhaps provide realistic mechanical boundary conditions for such a model. From a solution for this overall model, it would be possible to determine a possibly better "top-surface" boundary condition for the model of Figure 10 plus better tractions on the vertical surfaces there with some axial (z) variation.

Finally, the broader questions concerning the thermoelastic model itself, e.g. the questions of inelastic effects, low-cycle fatigue, crack propagation, temperature-dependent material properties, are all relevant to the described physical turbine blade configuration and should be addressed as feasible in future investigations.

ACKNOWLEDGEMENT

We gratefully acknowledge support of this investigation by the United States Air Force Office of Scientific Research under Grant No. AFOSR-75-2824. Special thanks are due Dr. Frank Sagendorph, General Electric Co., Evendale, Ohio for his interest and valuable contributions to the described research.

REFERENCES

1. Rizzo, F. J. and Shippy, D. J. "Thermomechanical Stress Analysis of Advanced Turbine Blade Cooling Configuration," AFOSR-TR-76-0841, May, 1976.

2. Rizzo, F. J. and Shippy, D. J. "Thermomechanical Stress Analysis of Advanced Turbine Blade Cooling Configuration," AFOSR-TR-77-0950, July 1977.

3. Rizzo, F. J. and Shippy, D. J. "Thermomechanical Stress Analysis of Advanced Turbine Blade Cooling Configuration," AFOSR Interim Report, July 1978.

4. Cruse, T. A. and Rizzo, F. J. (Eds.), "Boundary integral equation method: computational applications in applied mechanics", 1975, ASME Proc. AMD - Vol. 11, New York.

5. Rizzo, F. J. and Shippy, D. J., Int. J. Num. Meth. Engng. 1977, 11, 1753.

6. Boley, B. A. and Weiner, J. H., "Theory of thermal stresses", 1960, Wiley, New York.

7. Lachat, J. C., "A further development of the boundary integral technique for elastostatics", Dissertation, 1975, Univ. of Southampton, England.

8. Cruse, T. A. and Van Buren, W., Int. J. Frac. Mech. 1971, 7, 1.

9. Lachat, J. C. and Watson, J. O., Int. J. Num. Meth. Engng. 1976, 10, 991.

10. Stroud, A. H. and Secrest, D., "Gaussian Quadrature Formulas", 1966, Prentice-Hall, New York.

11. Lyness, J. N. and Jespersen, D., J. Inst. Maths. Applics. 1975, 15, 19.

12. Rizzo, F. J. and Shippy, D. J., "On the numerical integration of certain functions pertinent to the boundary integral method for three-dimensional elasticity", (in preparation).

13. Wu, Y. S., "The Boundary integral equation method using various approximation techniques for problems governed by Laplace's equation", Special Scientific Report AFOSR-TR-76-1313, 1976, Washington, D.C.

14. Fairweather, G., Rizzo, F. J., Shippy, D. J., Wu, Y. S., "On the numerical solution of two-dimensional potential problems by an improved boundary integral equation method", J. Comp. Phys. 1976, 31, 96.

15. Cruse, T. A. and Lachat, J. C. (Eds.), "Proceedings of the international symposium on innovative numerical analysis in applied engineering science", 1977 Versailles, France.

16. Brebbia, C. A. ed., "Recent advances in boundary element methods", 1978, Pentech Press, London.

APPENDIX

Fundamental Kernel Functions

i) $B \in E^3$

$$K = 1/r, \quad K' = \frac{\partial}{\partial n}(1/r)$$

$$U_{ij} = \frac{(1+\nu)}{8\pi E(1-\nu)} \left(\frac{1}{r}\right) [(3-4\nu)\delta_{ij} + r_{,i}r_{,j}]$$

$$T_{ij} = \frac{-(1-2\nu)}{8\pi(1-\nu)} \left(\frac{1}{r^2}\right) \left[\frac{\partial r}{\partial n}\{\delta_{ij} + \frac{3}{(1-2\nu)} r_{,i}r_{,j}\} + r_{,i}n_j - r_{,j}n_i\right]$$

$$W = \frac{(1-2\nu)(1+\nu)}{8\pi E(1-\nu)} r$$

ii) $B \in E^2$ (plane strain)

$$K = -\log r, \quad K' = -\frac{\partial}{\partial n} \log r$$

$$U_{ij} = \frac{-(1+\nu)}{4\pi E(1-\nu)} [(3-4\nu) \log r\, \delta_{ij} - r_{,i}r_{,j}]$$

$$T_{ij} = \frac{-(1-2\nu)}{4\pi(1-\nu)} \left[\frac{\partial}{\partial n} \log r \{\delta_{ij} + \frac{2}{(1-2\nu)} r_{,i}r_{,j}\} + (\log r)_{,i}n_j - (\log r)_{,j}n_i\right]$$

$$W = \frac{-(1-2\nu)(1+\nu)}{8\pi E(1-\nu)} r^2 (\log r - 1)$$

Material Parameters

E is Young's Modulus, ν is Poisson's Ratio

k_o is the Laplacian of the Body Force Potential

$\gamma \equiv E\alpha/(1-2\nu)$, α is the coefficient of Thermal Expansion

Shape Functions

i) Quadrilateral

$$M_R^1 = \frac{1}{4}(\xi_1 + 1)(\xi_2 + 1)(\xi_1 + \xi_2 - 1), \quad M_R^5 = \frac{1}{2}(\xi_1 + 1)(1 - \xi_2^2)$$

$$M_R^2 = \frac{1}{4}(\xi_1 - 1)(\xi_2 + 1)(\xi_1 - \xi_2 + 1), \quad M_R^6 = \frac{1}{2}(\xi_2 + 1)(1 - \xi_1^2)$$

$$M_R^3 = \frac{1}{4}(1 - \xi_1)(\xi_2 - 1)(\xi_1 + \xi_2 + 1), \quad M_R^7 = \frac{1}{2}(\xi_1 - 1)(\xi_2^2 - 1)$$

$$M_R^4 = \frac{1}{4}(\xi_1 + 1)(\xi_2 - 1)(\xi_2 - \xi_1 + 1), \quad M_R^8 = \frac{1}{2}(1 - \xi_2)(1 - \xi_1^2)$$

ii) Triangular

$$M_T^1 = \xi_1(2\xi_1 - 1), \quad M_T^4 = 4\xi_1\xi_3$$

$$M_T^2 = \xi_2(2\xi_2 - 1), \quad M_T^5 = 4\xi_1\xi_2 \qquad \xi_1 + \xi_2 + \xi_3 = 1$$

$$M_T^3 = \xi_3(2\xi_3 - 1), \quad M_T^6 = 4\xi_2\xi_3$$

iii) One-Dimensional

$$M^1 = -\frac{1}{2}(\xi - \xi^2), \quad M^2 = 1 - \xi^2, \quad M^3 = \frac{1}{2}(\xi + \xi^2)$$

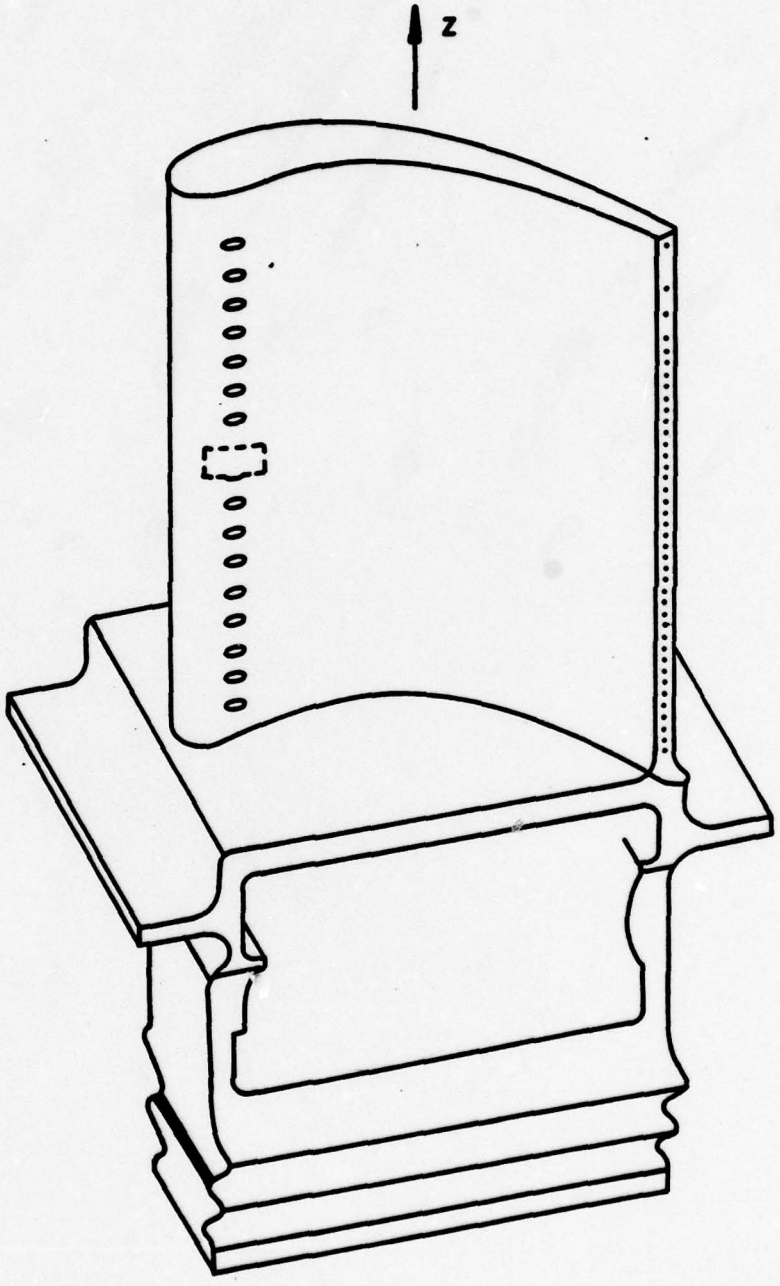

Figure 1. Schematic Drawing of Typical Turbine Blade

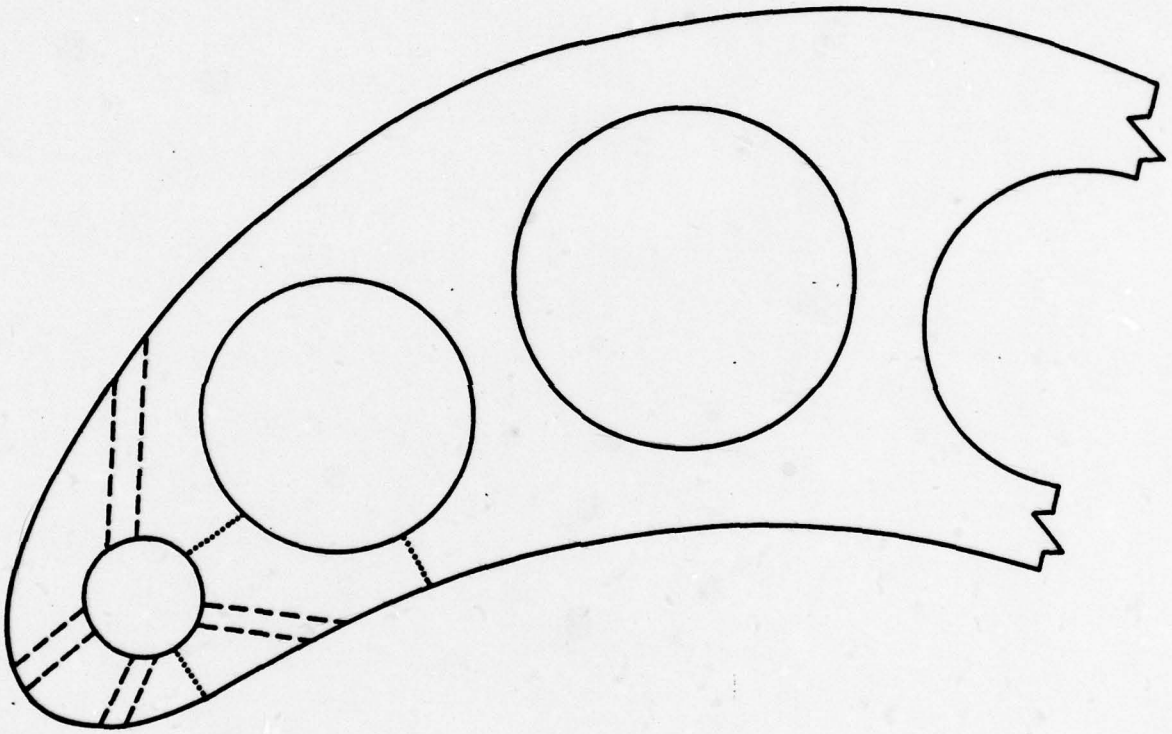

Figure 2. Cross-Section of Turbine Blade

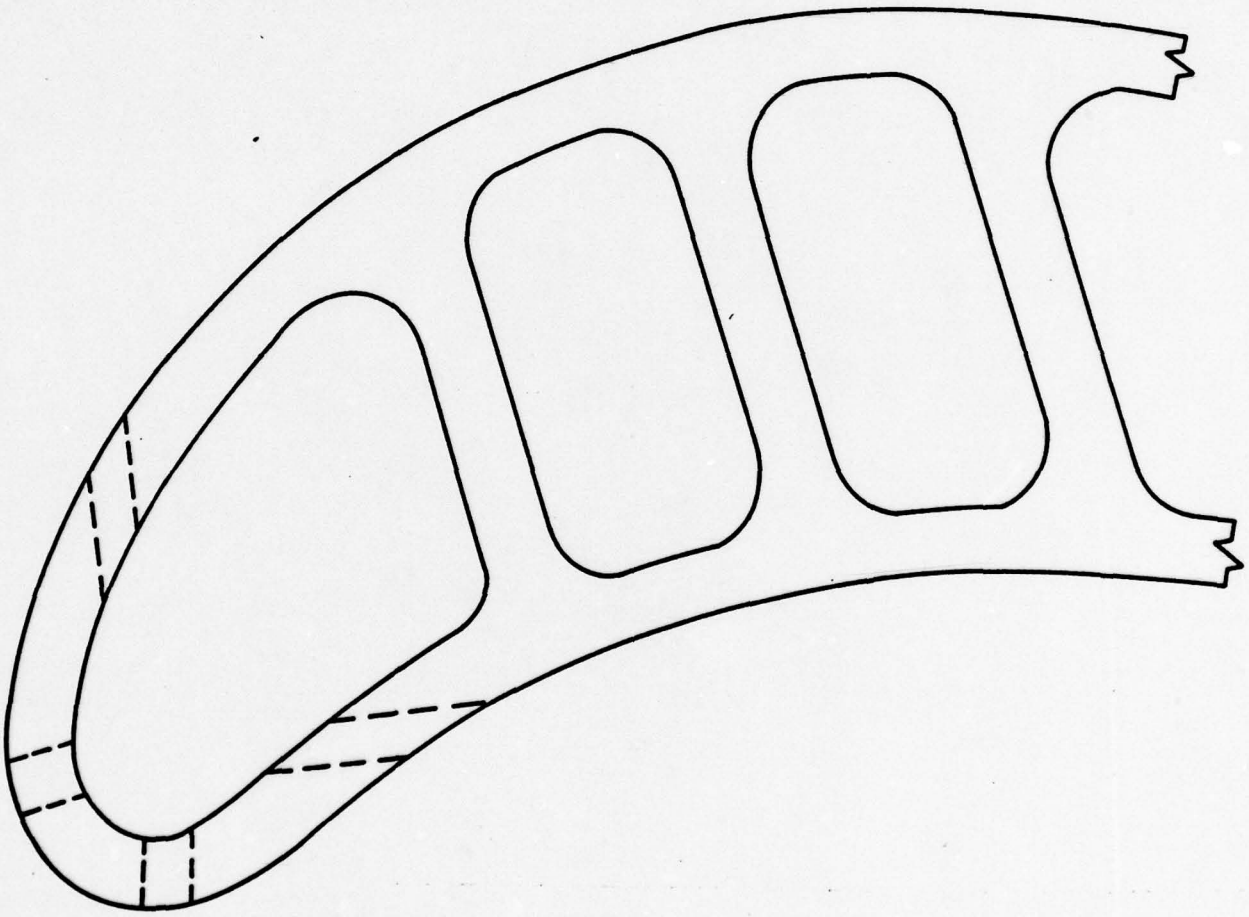

Figure 3. Cross-Section of Turbine Blade

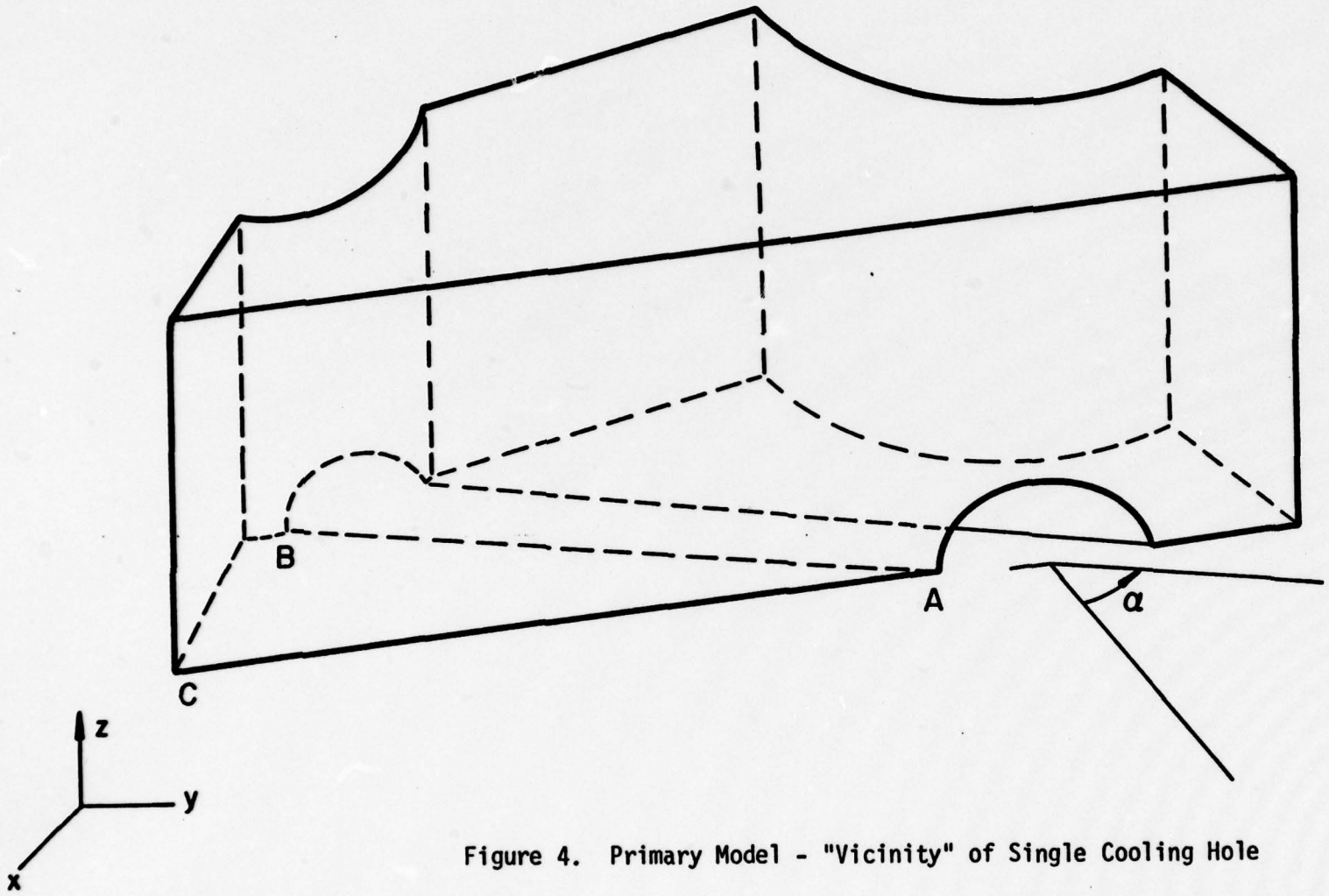

Figure 4. Primary Model - "Vicinity" of Single Cooling Hole

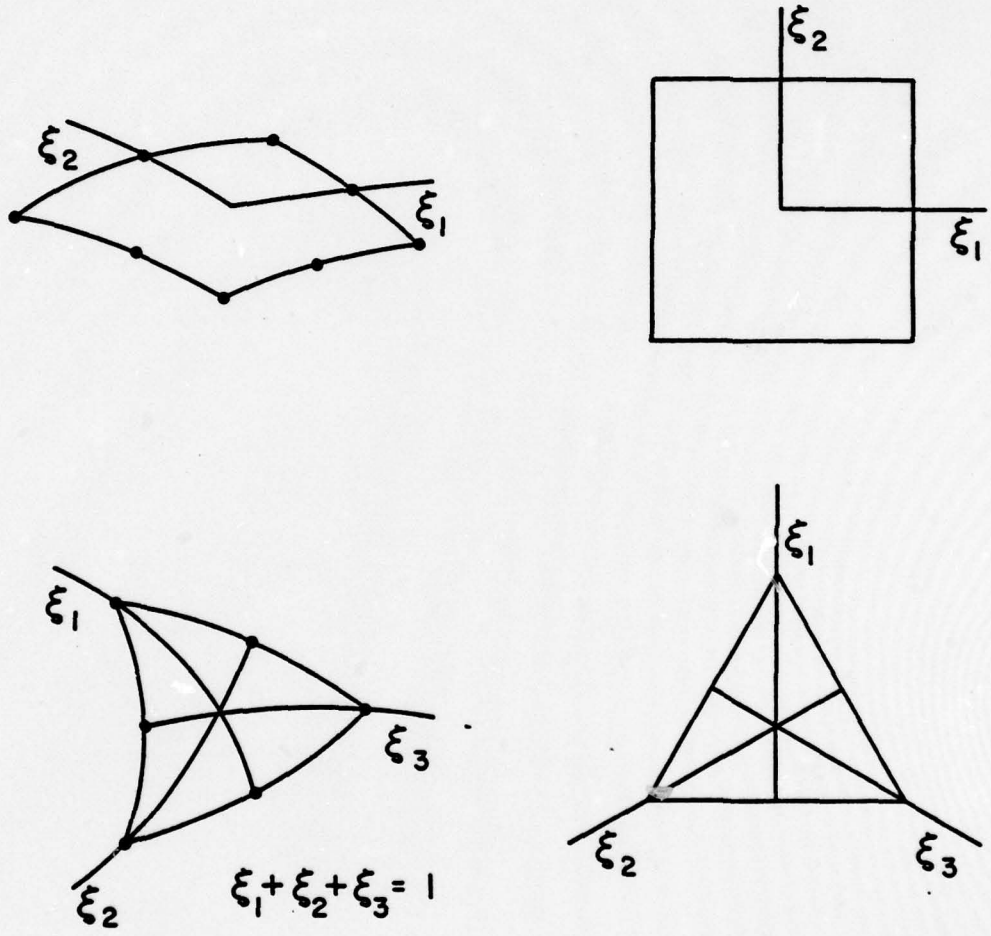

Figure 5. Quadrilateral and Triangular Surface Elements

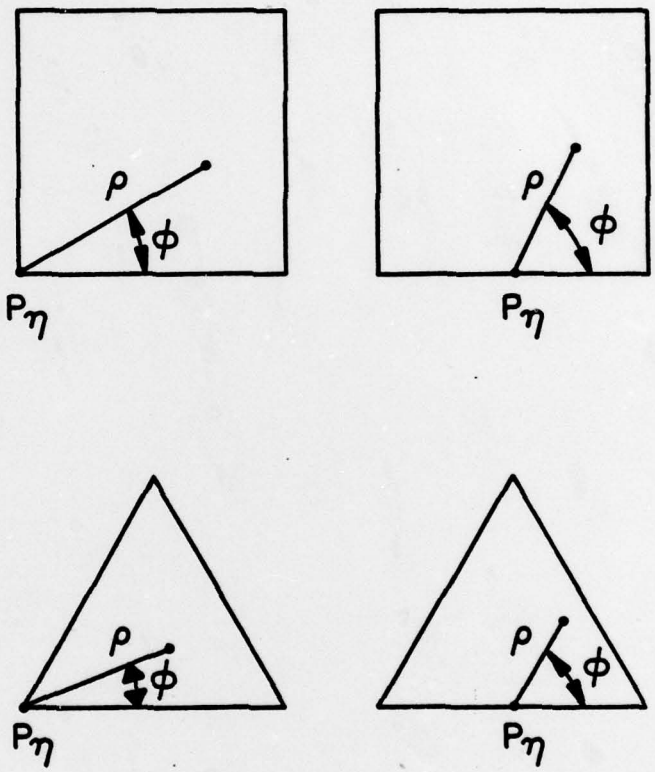

Figure 6. Polar Coordinate System for Case when $P_\eta \in S_\sigma$

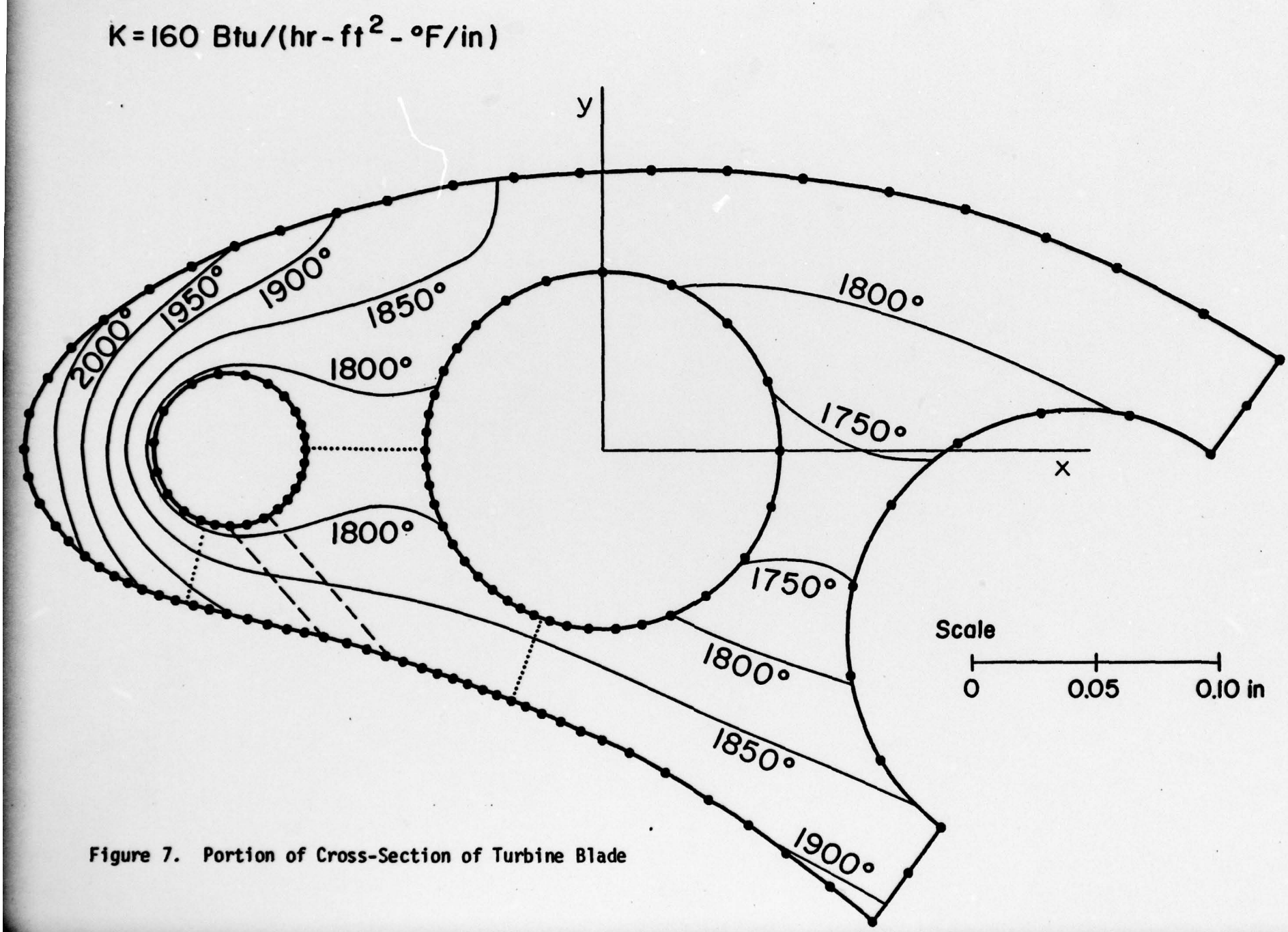

Figure 7. Portion of Cross-Section of Turbine Blade

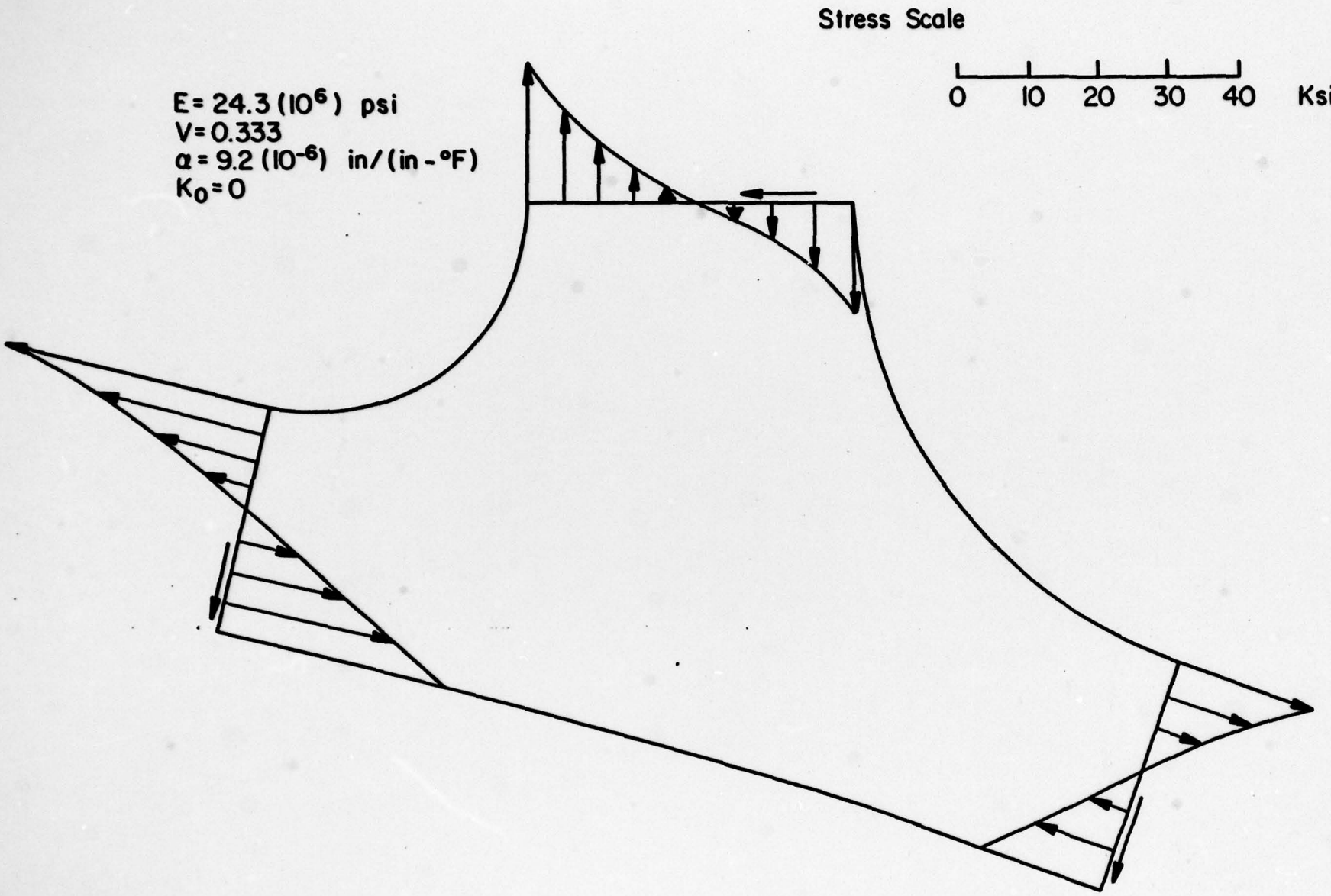

Figure 8. Thermal Stress Distribution on Piece of Turbine Blade

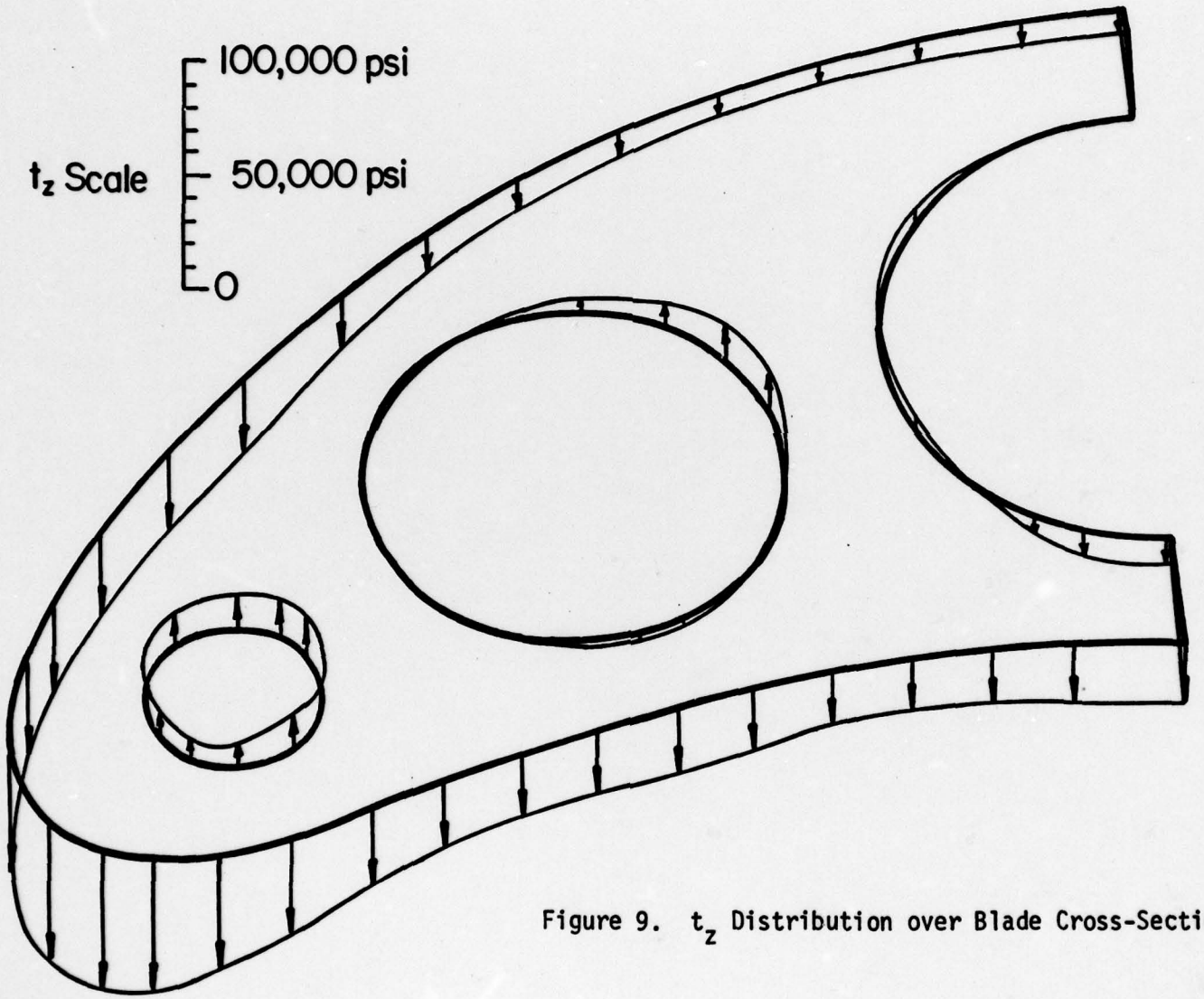

Figure 9. t_z Distribution over Blade Cross-Section

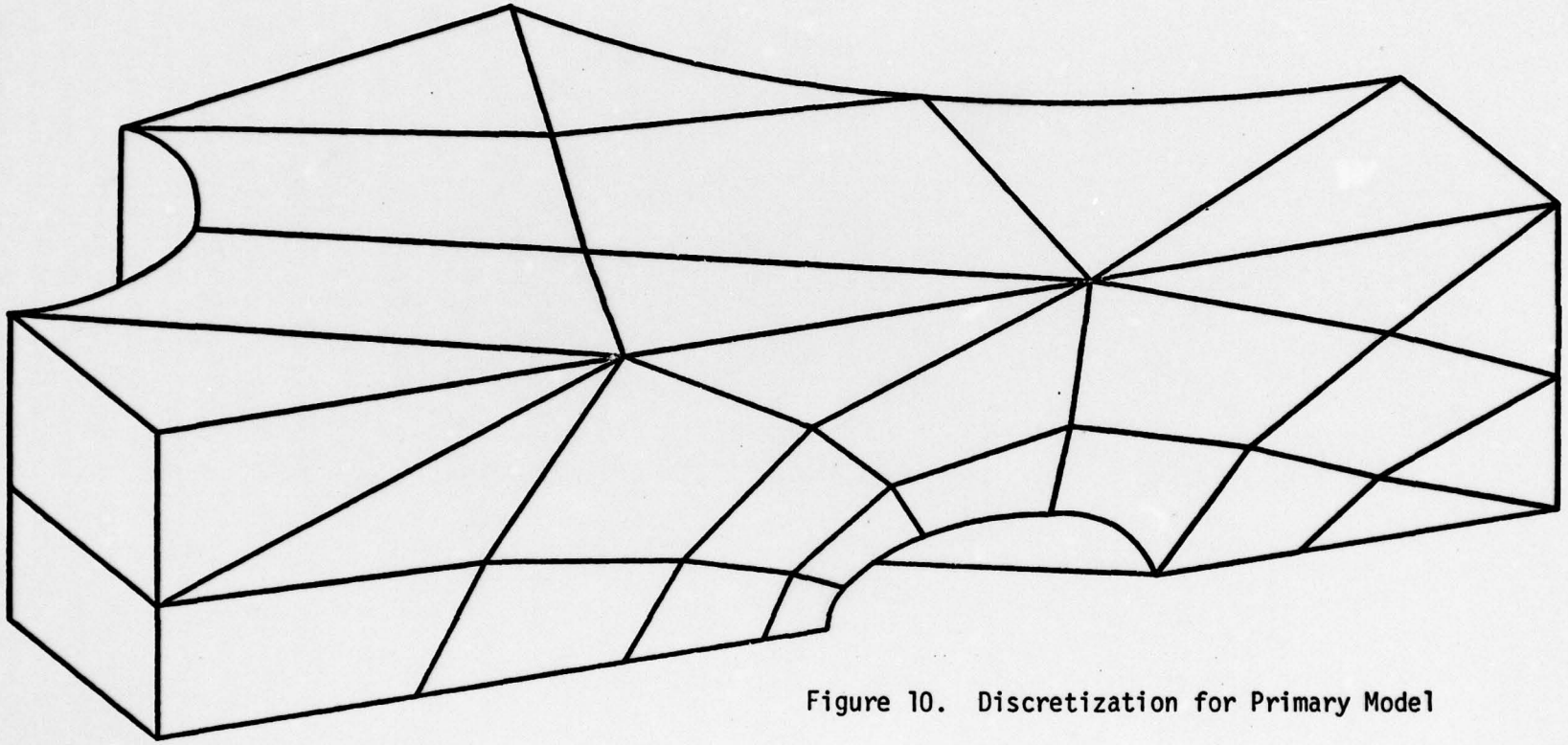

Figure 10. Discretization for Primary Model

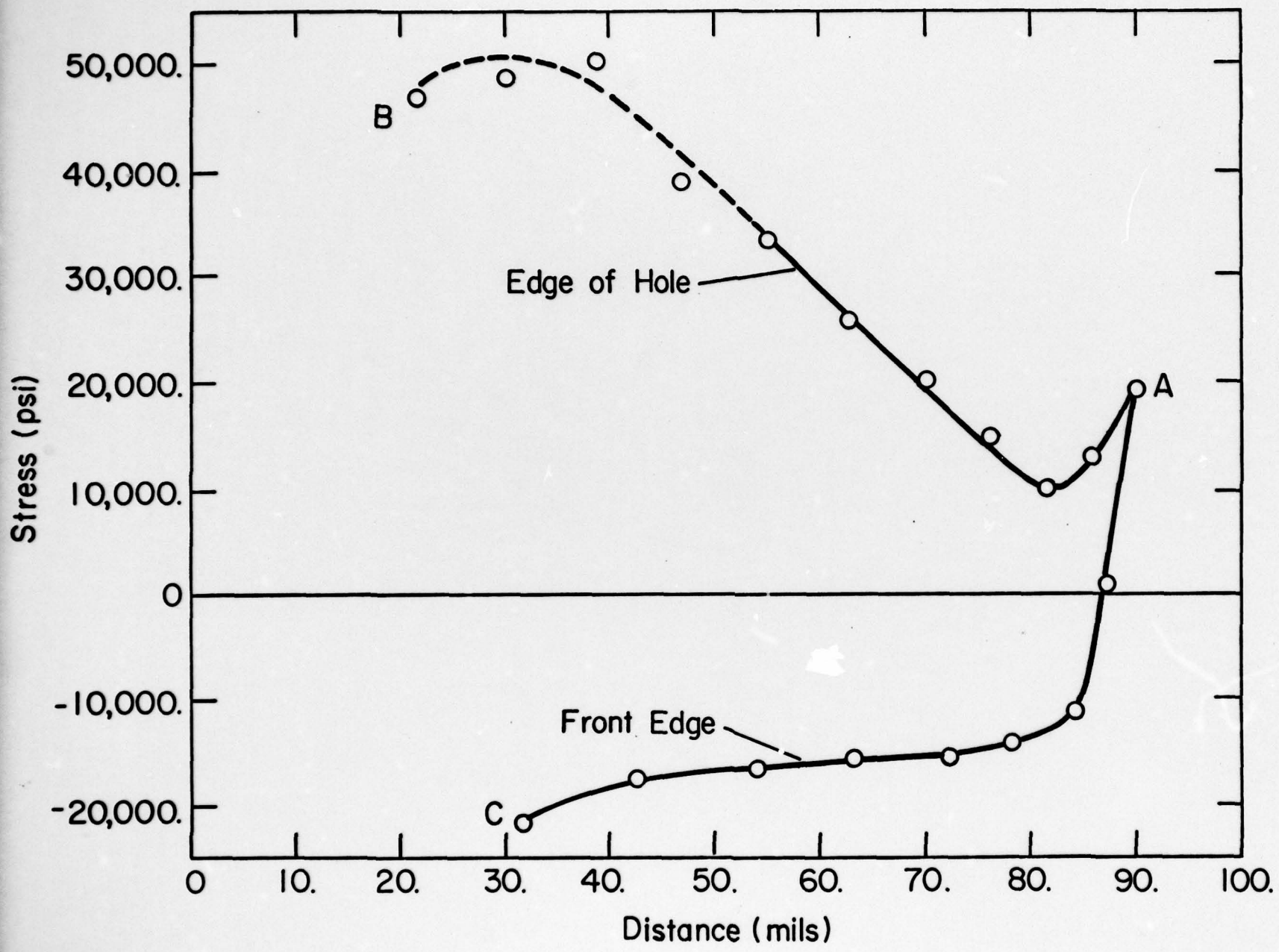

Figure 11. Stress Distribution for Full Thermoelastic Problem

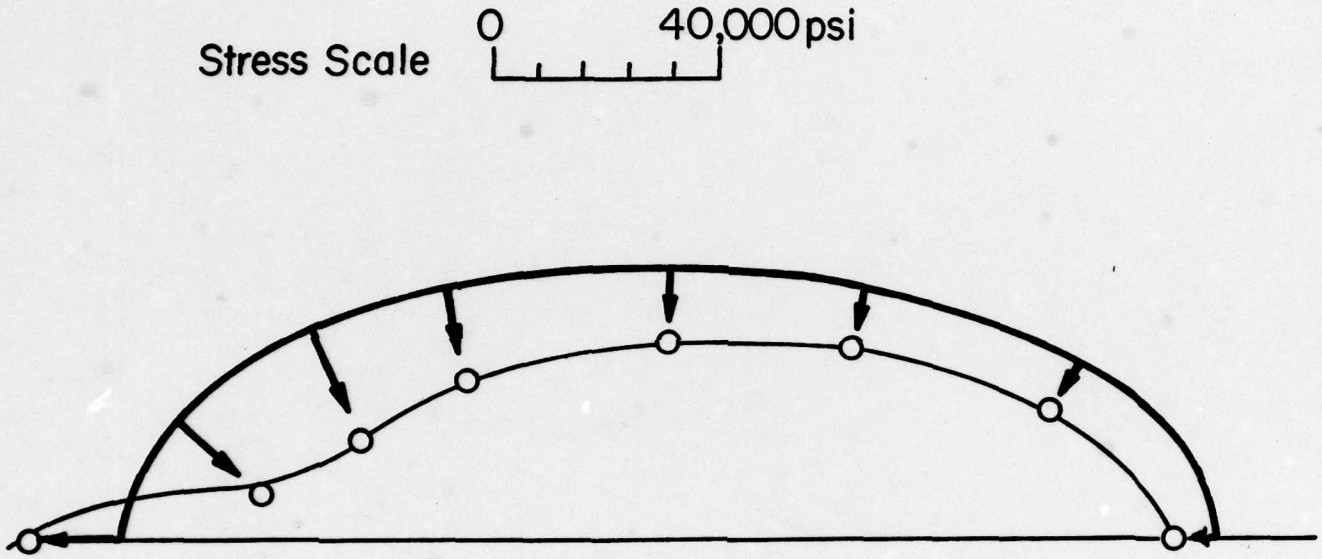

Figure 12. Hoop Stress Pattern for Full Thermoelastic Problem

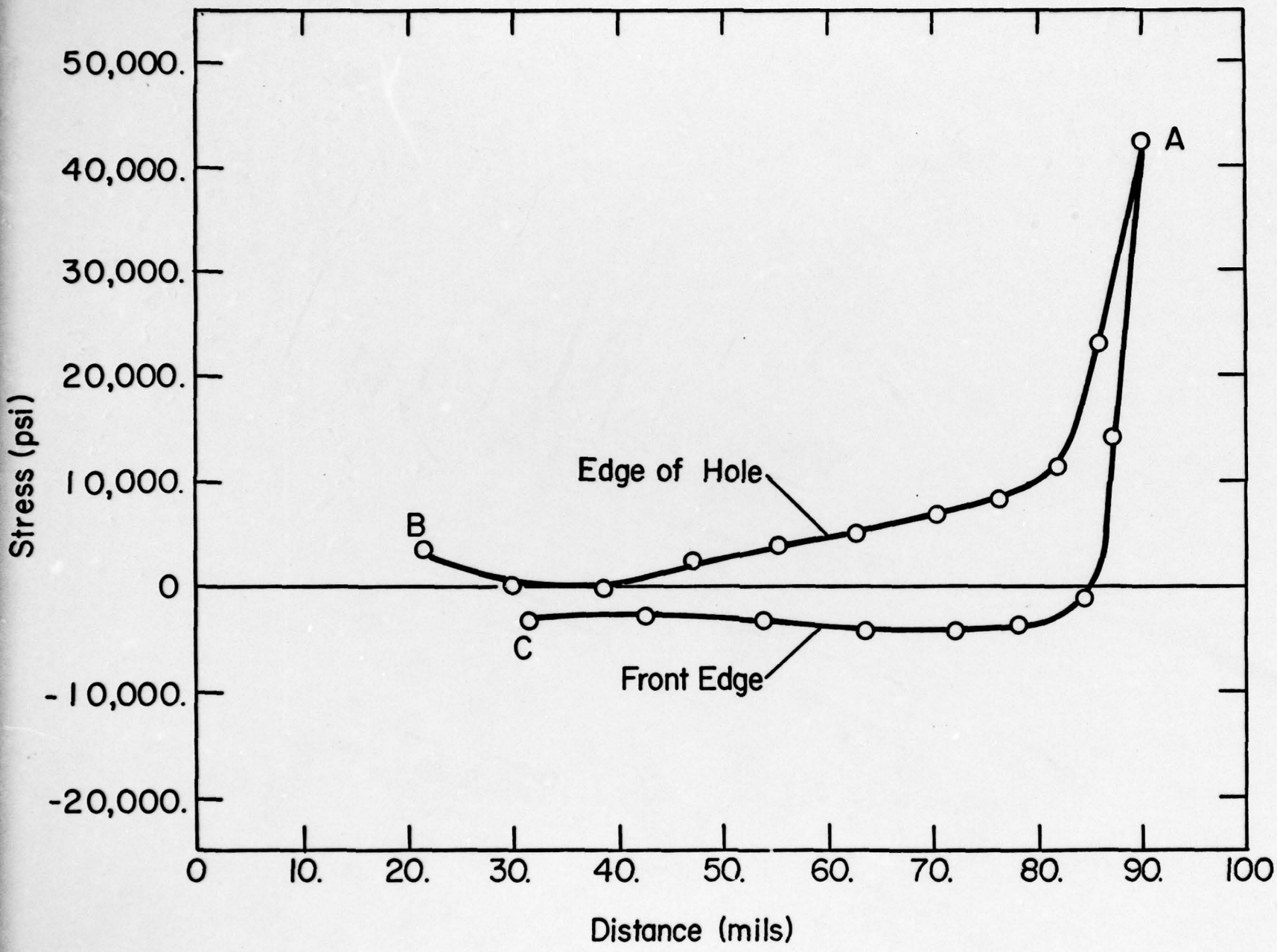

Figure 13. Stress Distribution for Component Problem (i)

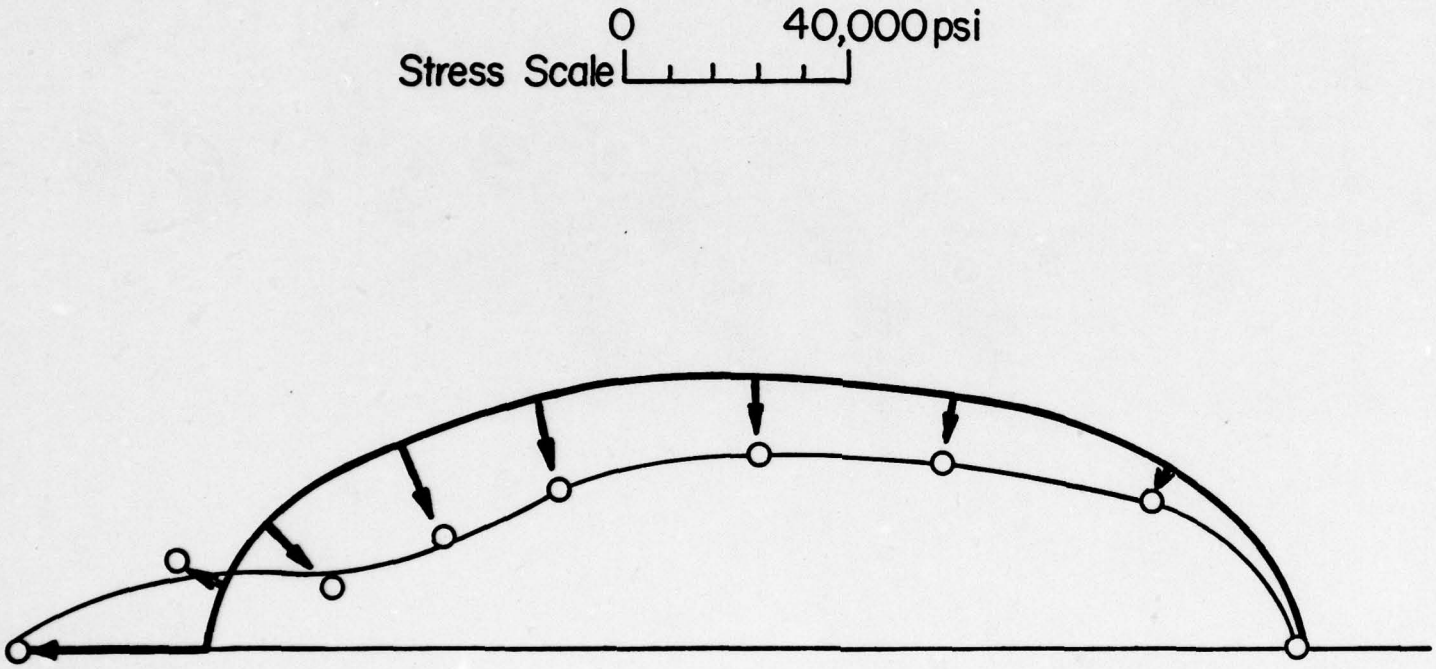

Figure 14. Hoop Stress Pattern for Problem (i)

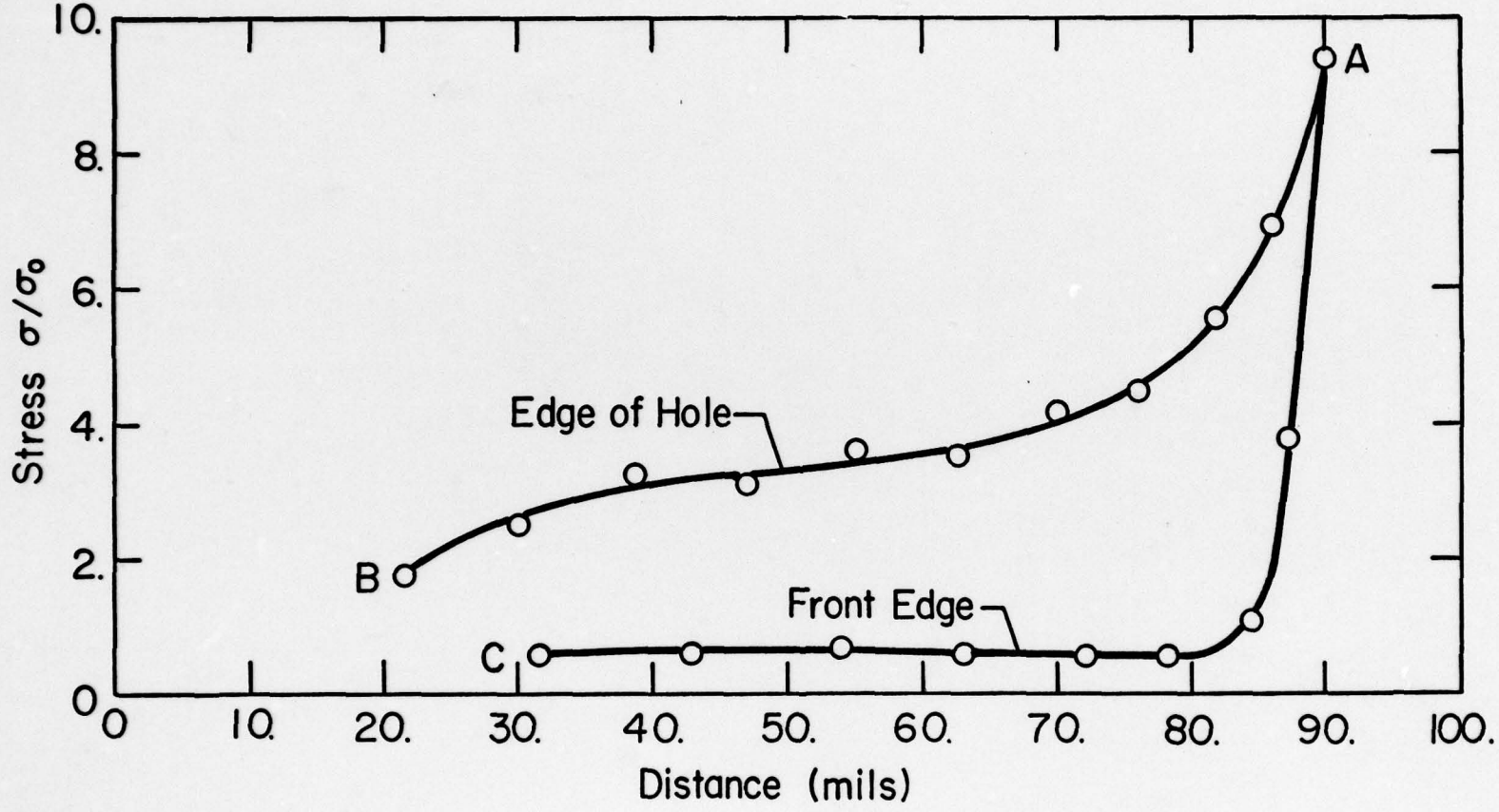

Figure 15. Stress Distribution for Centrifugal Input $\sigma_0 = 1$

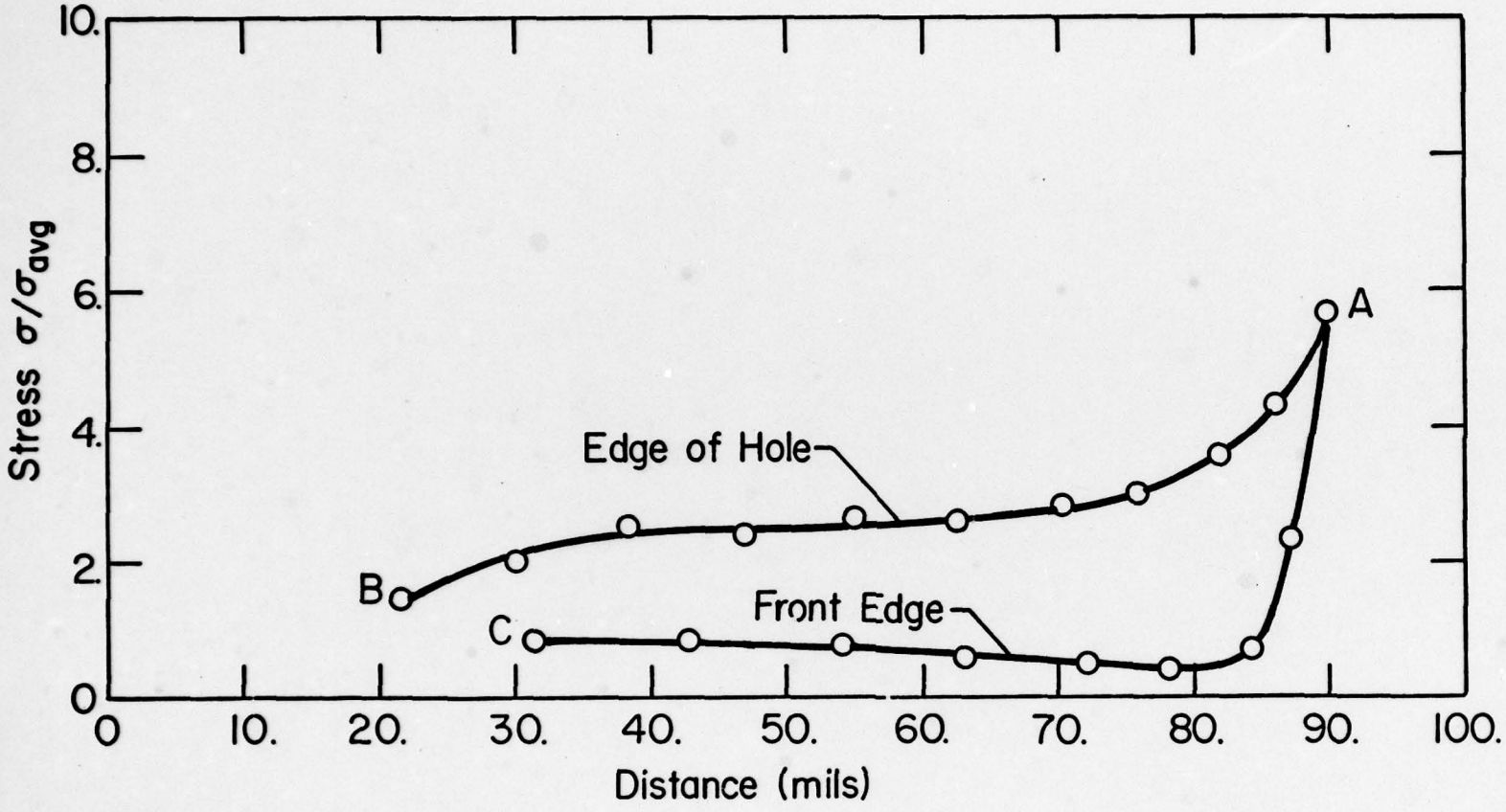

Figure 16. Stress Distribution for Centrifugal Input $u_o = 1$

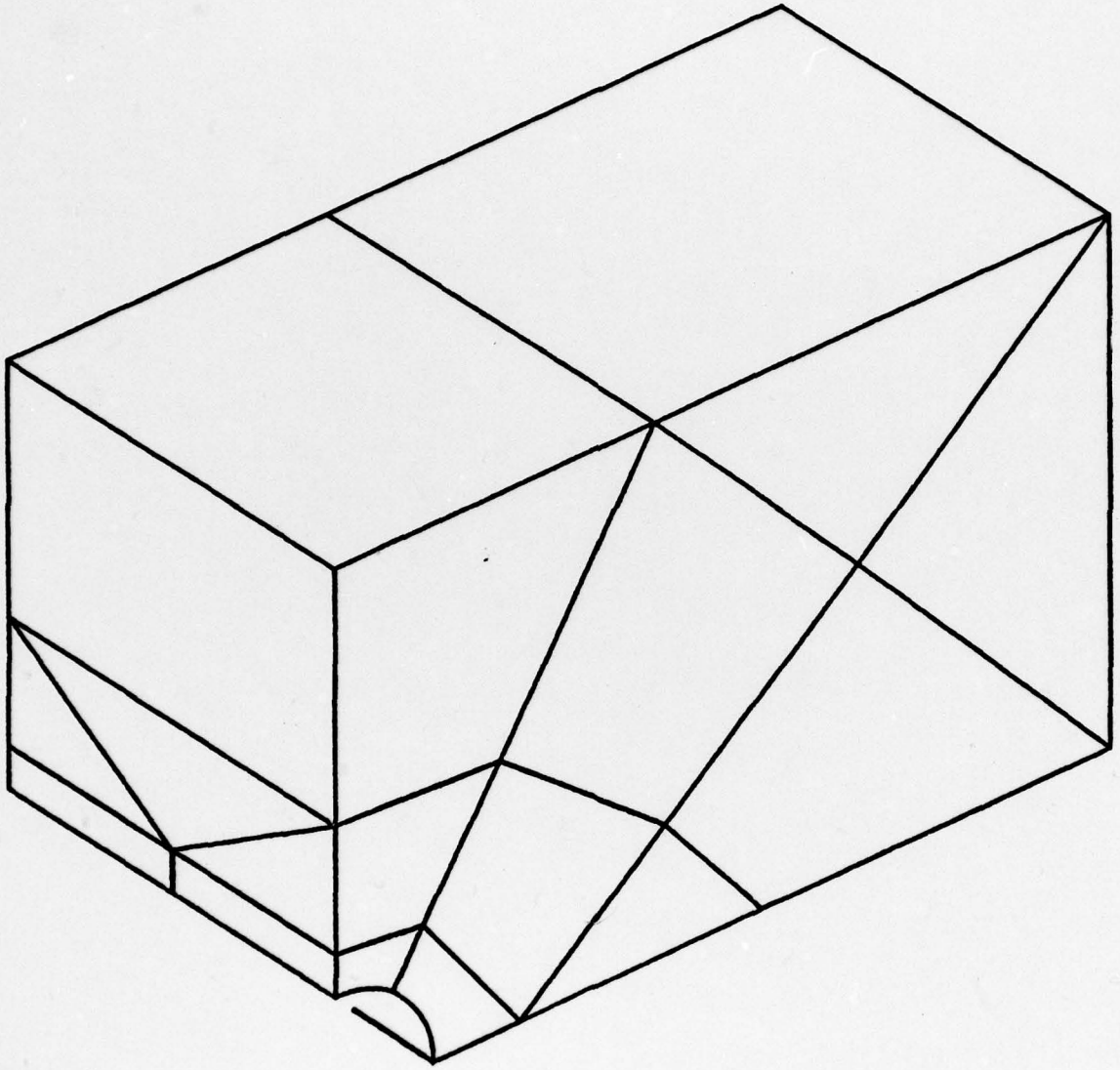

Figure 17. Discretization of Plate with Straight-Thru-Hole

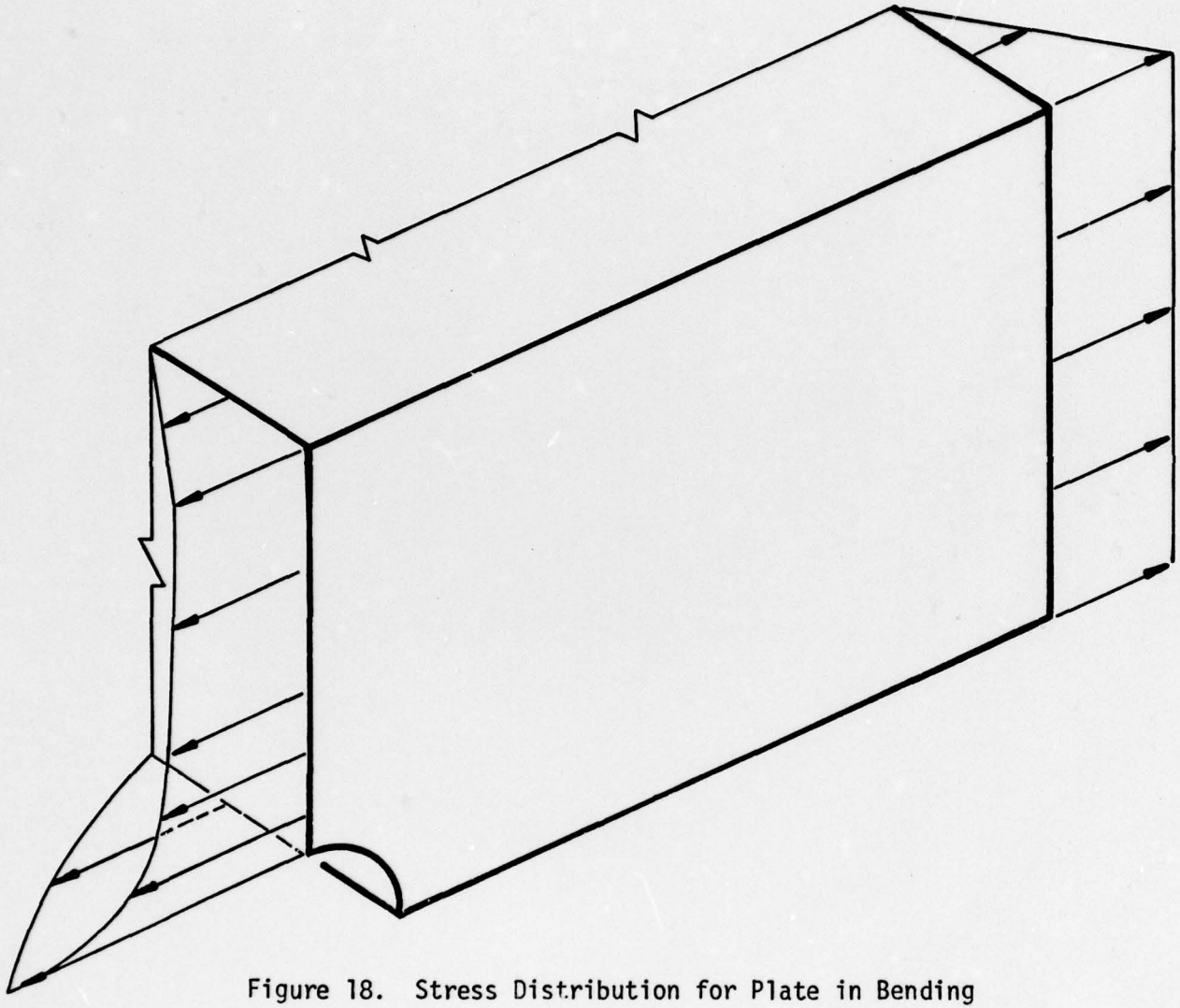

Figure 18. Stress Distribution for Plate in Bending

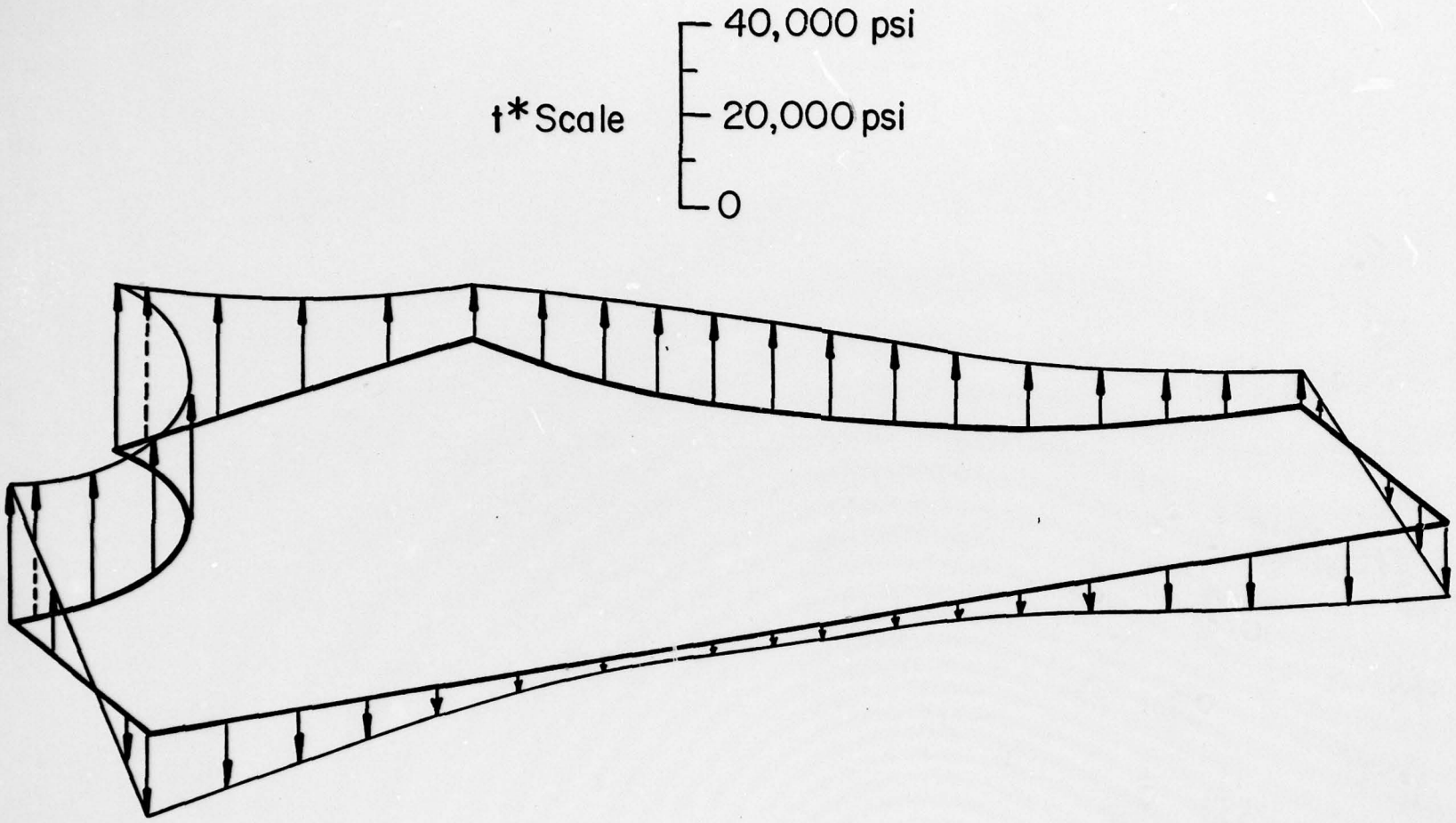

Figure 19. t^* Distribution over Top of Primary Model